Draft version March 6, 2019
Typeset using LaTeX **twocolumn** style in AASTeX61

ROTATION PERIOD EVOLUTION IN LOW-MASS BINARY STARS: THE IMPACT OF TIDAL TORQUES AND MAGNETIC BRAKING

David P. Fleming,[1,2] Rory Barnes,[1,2] James R. A. Davenport,[1] and Rodrigo Luger[3,2]

[1] *Astronomy Department, University of Washington*
Box 951580, Seattle, WA 98195
[2] *NASA Astrobiology Institute - Virtual Planetary Laboratory Lead Team, USA*
[3] *Center for Computational Astrophysics, Flatiron Institute*
New York, NY 10010

(Received xxx; Revised yyy; Accepted zzz)

Submitted to AAS Journals

ABSTRACT

We examine how tides, stellar evolution, and magnetic braking shape the rotation period (P_{rot}) evolution of low-mass stellar binaries up to orbital periods (P_{orb}) of 100 d across a wide range tidal dissipation parameters using two common equilibrium tidal models. We find that many binaries with P_{orb} $\lesssim$20 d tidally-lock, and most with $P_{orb} \lesssim$4 d tidally-lock into synchronous rotation on circularized orbits. At short P_{orb}, tidal torques produce a population of fast rotators that single-star only models of magnetic braking fail to produce. In many cases, we show that the competition between magnetic braking and tides produces a population of subsynchronous rotators that persists for Gyrs, even in short P_{orb} binaries, qualitatively reproducing the subsynchronous eclipsing binaries (EBs) discovered in the *Kepler* field by Lurie et al. (2017). Both equilibrium tidal models predict that binaries can tidally-interact out to $P_{orb} \approx 80$ d, while the CPL equilibrium tidal model predicts that binaries can tidally-lock out to $P_{orb} \approx 100$ d. Tidal torques often force the P_{rot} evolution of stellar binaries to depart from the long-term magnetic braking-driven spin down experienced by single stars, revealing that P_{rot} is not be a valid proxy for age in all cases, i.e. gyrochronology methods can fail unless one accounts for binarity. We suggest that accurate determinations of orbital eccentricities and P_{rot} can be used to discriminate between which equilibrium tidal models best describes tidal interactions in low-mass binary stars.

Keywords: binaries: close, stars: evolution, stars: kinematics and dynamics, stars: rotation

1. INTRODUCTION

The long-term angular momentum evolution of low-mass (M $\lesssim$1 $M_{\odot}$) stars is controlled by magnetic braking, the torque exerted on stars due to the coupling of stellar winds to the surface magnetic field (Dunn 1961; Mestel 1968). Early in stellar lifetimes, stars spin-up as they contract along the pre-main sequence. Once stars reach the main sequence, stellar radii remain mostly constant while magnetic braking removes angular momentum from the stars, gradually spinning them down over time (Skumanich 1972). Although the precise details of how magnetic braking operates are not fully known, models of magnetic braking have been used to successfully model the bulk trends of P_{rot} distributions in clusters (e.g. Praesepe, Matt et al. 2015; Douglas et al. 2017) and field stars (e.g. the *Kepler* field, Reiners & Mohanty 2012; Matt et al. 2015; van Saders et al. 2018). Furthermore, the magnetic braking-driven long-term spin-down of stars has been used to estimate stellar ages, a method known as gyrochronlogy (Skumanich 1972; Barnes 2003, 2007; Mamajek & Hillenbrand 2008; Barnes 2010), with older stars assumed to have lost more angular momentum due to magnetic braking and therefore rotate more slowly.

In contrast, the angular momentum evolution in low-mass short-period (P_{orb} $\lesssim$10 d) stellar binaries is dominated by tides. Tidal torques drive secular changes in the binary orbit and stellar spins, eventually circularizing the orbit and synchronizing the stellar spins in the long-term (Counselman 1973). Orbital circularization is ubiquitous for short-period binaries, owing to the tidal torque's strong radius and semi-major axis dependence, with both theoretical (e.g. Zahn & Bouchet 1989; Claret et al. 1995) and observational (e.g. Meibom & Mathieu 2005; Mazeh 2008; Lurie et al. 2017) studies finding that most binaries with P_{orb} $\lesssim$10 d are circularized. For short-period binaries, tidal torques work quickly on $\sim$100 Myr timescales, as Zahn & Bouchet (1989) found that the orbit of solar twin binaries circularize during the stellar pre-main sequence. Observations by Meibom & Mathieu (2005) support this picture as they find short-period binaries in the $\sim$150 Myr old cluster M35 tend to have circular orbits.

Tides impart a significant signature in the long-term angular momentum evolution for binary stars, especially for stellar spins. Tidal torques drive binaries towards the tidally-locked state in which the stellar P_{rot} is equal to the equilibrium rotation period (P_{eq}) predicted by tidal models, with a familiar example of this effect being spin-orbit synchronization where $P_{rot} = P_{eq} = P_{orb}$. Tidal-locking occurs much earlier than orbital circularization with the tidal-locking timescale estimated to be $2 - 3$ orders of magnitude less than the circularization timescale (Zahn & Bouchet 1989; Witte & Savonije 2002; Mazeh 2008) as there is typically much less angular momentum in stellar spins than the binary orbit. As a result, tidal-locking is expected for binaries with $P_{orb} \lesssim$ 20 d (e.g. Levato 1974; Meibom et al. 2006; Mazeh 2008; Zahn 2008; Meibom et al. 2015).

In low-mass binaries, both magnetic braking and tidal torques compete to shape the stellar P_{rot} evolution. When tides dominate, in particular at close orbital separations, tides can fix $P_{rot} = P_{orb}$, or more generally $P_{rot} = P_{eq}$ for eccentric orbits. In such situations, magnetic braking still operates, removing angular momentum from each star, forcing tides to compensate for each star's loss of angular momentum by spinning up the stars to maintain the tidally-locked equilibrium, removing angular momentum from the orbit, hardening the binary (Verbunt & Zwaan 1981; Repetto & Nelemans 2014; Fleming & Quinn 2017). Tides do not win out over magnetic braking in general, however, as magnetic braking can spin-down the stars past the tidally-locked state into subsynchronous rotation (e.g. $P_{rot} > P_{eq}$, Habets & Zwaan 1989; Zahn 1994; Keppens 1997). This behavior seems to be bourne out in nature, as Lurie et al. (2017) discovered a substantial population of subsynchronous short-period binaries in the *Kepler* field, clustered near $P_{orb}/P_{rot}$$\approx$0.9, in defiance of the expectation of tidal locking at such short orbital separations.

The influence of tides is not necessarily limited to short P_{orb} systems, as Abt & Boonyarak (2004) found that the P_{rot} evolution of stellar binaries out to $P_{orb} \approx$ 500 d can deviate from that of single stars, meriting the examination of the impact of tides out to longer P_{orb} than is traditionally considered. The competition between magnetic braking and tidal torques can lead to complex angular momentum evolution in low-mass stellar binaries, and no previous work has conducted a systematic study to examine how this evolution proceeds across a wide range of tidal dissipation parameters and P_{orb}.

Understanding the interaction between tidal torques and magnetic braking is of paramount importance as P_{rot} distributions measured in clusters (e.g. Praesepe, Agüeros et al. 2011; Douglas et al. 2017) and field stars (e.g. *Kepler*, Reinhold et al. 2013; McQuillan et al. 2014) are likely contaminated by unresolved binaries given that roughly half of Sun-like stars are in stellar binaries (Raghavan et al. 2010; Duchêne & Kraus 2013), and that binaries are difficult to resolve in photometric surveys. In the *Kepler* field, for example, Simonian et al. (2018) recently found that most rapid rotators (P_{rot} $\lesssim$7.5 d) are likely non-eclipsing, tidally-synchronized short-period photometric binaries, indicating that tidal torques in binaries can significantly impact observed P_{rot} distributions. Tidal torques can modify stellar rotation periods towards the tidally-locked state, away from the long-term spin-down due to magnetic braking predicted for single stars (Dunn 1961; Skumanich 1972; Barnes 2003), or compete against magnetic braking to form subsychronous rotators, imparting a contaminating signal that is not currently accounted for by models. Moreover, any ages inferred from rotation periods of stars in unresolved binaries using gyrochronology could be incorrect owing to the influence of tidal torques. No previous study has quantified this effect.

There is currently a large number of *Kepler* binaries with known P_{rot} and P_{orb} (e.g. Lurie et al. 2017). Both the extended *Kepler* mission (K2, Howell et al. 2014) and the Transiting Exoplanet Survey Satellite (TESS, Ricker et al. 2014; Sullivan et al. 2015) are expected to detect additional low-mass eclipsing binaries, with Gaia parallaxes (Gaia Collaboration et al. 2016) poised to help refine these stellar parameters, potentially creating a rich dataset of the angular momentum budgets of low-mass binaries. Developing a framework for the angular momentum evolution of low-mass binaries can enable the characterization of the nature of tidal torques in binaries by conditioning on datasets of the spin and orbital states of stellar binaries.

Here, we present a model for the angular momentum evolution of low-mass stellar binaries over their full pre-main and main sequence lifetimes using a realistic treatment of stellar evolution, magnetic braking, and tidal torques. We investigate under what conditions tidal-locking occurs, and how tidal torques influence rotation in stellar binaries as a function of binary P_{orb} and tidal dissipation parameters for two widely-used equilibrium tidal models and two magnetic braking models. We show how tidal torques can impact stellar rotation in binaries out to $P_{orb} = 100$ d, causing stellar rotation periods to not strongly correlate with age, making the predictions of gyrochronlogy models to potentially fail in such systems. We describe our model in § 2 and our simulation procedure in § 3. We discuss our results in § 4, apply our model to the *Kepler* field in § 4.5, and discuss our results' implications in § 5.

2. METHODS

We simulate coupled stellar-tidal evolution for low-mass binaries using an improved version of the model presented in Fleming et al. (2018). We implement our model in the open-source code VPLanet[1] (Barnes et al. 2016, 2018, Barnes et al., in prep). We integrate all model equations (see § 2.1 and § 2.2) using using the 4^{th} order Runge-Kutta scheme with adaptive timestepping described in Fleming et al. (2018).

2.1. *Stellar Evolution*

We improve upon the stellar evolution model used in Fleming et al. (2018), STELLAR, by tracking the evolution of both the stellar radius of gyration, r_g, and radius, R, using a bicubic interpolation over mass and time of the Baraffe et al. (2015) stellar evolution models. We consider two separate magnetic braking models to gauge how sensitive the interaction between tides and magnetic braking is in modifying P_{rot} evolution in stellar binaries.

The first magnetic braking model we use was derived by Matt et al. (2015) and has been shown to successfully model the spin-down of low-mass stars across many ages in both the Praesepe cluster and in the *Kepler* field. This model is strongly dependent on the stellar Rossby number, $Ro = P_{rot}/\tau_{cz}$, the ratio of the stellar P_{rot} to the stellar convective turnover timescale, τ_{cz}. The Matt et al. (2015) model predicts that below a certain Ro for rapidly rotating stars, stellar magnetic activity saturates at a constant value, producing a magnetic braking torque that is directly proportional to the stellar rotation rate. The angular momentum loss for rapidly-rotating saturated stars is given by

$$\frac{dJ}{dt} = -\left.\frac{dJ}{dt}\right|_0 \chi^2 \left(\frac{\omega}{\omega_\odot}\right) \tag{1}$$

while for more slowly-rotating unsaturated stars,

$$\frac{dJ}{dt} = -\left.\frac{dJ}{dt}\right|_0 \left(\frac{\tau_{cz}}{\tau_{cz\odot}}\right)\left(\frac{\omega}{\omega_\odot}\right)^3 \tag{2}$$

where

$$\left.\frac{dJ}{dt}\right|_0 = 9.5\times10^{30} \text{ erg } \left(\frac{R}{R_\odot}\right)^{3.1}\left(\frac{M}{M_\odot}\right)^{0.5}. \tag{3}$$

Saturated magnetic braking occurs for $Ro \leq Ro_\odot/\chi$ for $\chi = 10$ where Matt et al. (2015) defines $\chi = Ro_\odot/Ro_{sat}$. We adopt all model parameters given in Table 1 from Matt et al. (2015) and compute τ_{cz} using Eqn. (36) from Cranmer & Saar (2011).

The second model we consider was developed by Reiners & Mohanty (2012), who modeled stellar spin-down

[1] VPLanet is publicly available at https://github.com/VirtualPlanetaryLaboratory/vplanet.

as a function stellar magnetic field strength. Similar to the Matt et al. (2015) model, Reiners & Mohanty (2012) posit that magnetic braking can be divided into a unsaturated ($\omega < \omega_{crit}$) and unsaturated ($\omega \geq \omega_{crit}$) regime as follows:

$$\begin{aligned}\frac{dJ_\star}{dt} &= -C\left[\omega\left(\frac{R^{16}}{M^2}\right)^{1/3}\right] \text{ for } \omega \geq \omega_{crit}\\ \frac{dJ_\star}{dt} &= -C\left[\left(\frac{\omega}{\omega_{crit}}\right)^4 \omega\left(\frac{R^{16}}{M^2}\right)^{1/3}\right] \text{ for } \omega < \omega_{crit}.\end{aligned} \tag{4}$$

Reiners & Mohanty (2012) tuned their model to match the Sun's P_{rot} and the distribution of P_{rot} of Gyr-old low-mass field stars and find $C = 2.66 \times 10^3$ (gm^5 cm^{-10} s^3)$^{1/3}$, $\omega_{crit} = 8.56 \times 10^{-6}$ s^{-1} for $M > 0.35$ M$_\odot$, and for late M dwarfs with $M \leq 0.35 M_\odot$, $\omega_{crit} = 1.82 \times 10^{-6}$ s^{-1}.

We model the net change in the stellar rotation rate due to stellar evolution and magnetic braking via the following equation

$$\dot{\omega} = \frac{\dot{J}_{mb}}{I} - \frac{2\dot{R}\omega}{R} - \frac{2\dot{r_g}\omega}{r_g} \tag{5}$$

where the moment of inertia $I = M r_g^2 R^2$, $\dot{J}_{mb}$ is the angular momentum loss due to magnetic braking, and the time derivatives of the stellar R and r_g are computed numerically using our interpolation of the Baraffe et al. (2015) stellar evolution grids.

In Fig. 1, we plot the evolution of R, r_g, and P_{rot} for 0.2 M$_\odot$, 0.7 M$_\odot$, and 1 M$_\odot$ mass stars, representing an M, K , and G dwarf, respectively, computed according to our stellar evolution model, `STELLAR`, using both magnetic braking models. We assume all stars have an initial $P_{rot} = 1$ d and have an initial age of 5 Myr. All stars' radii contract along the pre-main sequence, spinning the stars up (right panel). Once the stars reach the main sequence, their structure changes slowly, allowing magnetic braking to dominate the stellar angular momentum evolution, significantly spinning-down the stars over long timescales. Both magnetic braking models produce qualitatively similar P_{rot} evolution, with the Reiners & Mohanty (2012) predicting marginally stronger torques. The r_g evolution noticeably differs between the stars as the late M dwarf's (green) r_g varies little as it remains fully convective, while the K and G dwarf grow a radiative core while on the pre-main sequence, decreasing r_g until both reach the main sequence.

2.2. *Tidal Evolution*

Equilibrium tidal models, first introduced by Darwin (1880), track the secular evolution of an orbiter's semi-major axis, a, eccentricity, e, and the rotation rates, ω_i, and obliquities ψ_i, of both gravitating bodies due to tidal torques. Equilibrium tidal models assume that tidally-interacting bodies raise tidal bulges on their companions that remain offset from the line connecting the bodies' centers of mass due to friction within each body. This assumption is typically referred to as the "weak friction approximation" (Zahn 2008). The tidal bulges cause torques that permit the exchange of angular momentum between the orbit and both bodies' spins. Equilibrium tidal models are linear since they assume that the tidal waves that comprise the tidal bulge raised on a body are uncoupled. Under these assumptions, the tidal evolution is analogous to a driven, damped harmonic oscillator (Greenberg 2009). For low-mass stars, equilibrium tidal models assume that tidal forces primarily dissipate energy in the outer-convective regions via viscous turbulence (see Zahn 2008). Although simple, equilibrium tidal models have been used to model the secular orbital and rotation evolution of both Solar System bodies and exoplanets (e.g. Goldreich & Soter 1966; Jackson et al. 2009; Leconte et al. 2010; Heller et al. 2011; Barnes et al. 2013; Barnes 2017) and stellar binaries (e.g. Zahn & Bouchet 1989; Zahn 2008; Khaliullin & Khaliullina 2011; Repetto & Nelemans 2014; Fleming et al. 2018). We refer the reader to Barnes (2017) for an in-depth discussion of the assumptions and limitations of equilibrium tidal models. Here, we consider two common equilibrium tidal models to study the secular spin-orbital evolution of low-mass stellar binaries.

2.2.1. *Constant Phase Lag Model*

The "Constant Phase Lag" (CPL) (Ferraz-Mello et al. 2008; Heller et al. 2011) equilibrium tidal model assumes that the tidal torque on one body due to its companion arises from a linear combination of several discrete, uncoupled tidal bulges, each with its own associated frequency, that maintain a fixed phase offset with respect to the line connecting the two stars' centers of mass. We use the `EQTIDE` implementation of the CPL model in VPLanet following the derivation of Ferraz-Mello et al. (2008). The equations that govern the secular change in e and a are as follows:

$$\frac{de}{dt} = -\frac{ae}{8Gm_1m_2}\sum_{i=1}^{2} Z_{i,\mathrm{CPL}}\left(2\varepsilon_{0,i} - \frac{49}{2}\varepsilon_{1,i} + \frac{1}{2}\varepsilon_{2,i} + 3\varepsilon_{5,i}\right) \tag{6}$$

$$\frac{da}{dt} = \sum_{i=1}^{2}\frac{da_i}{dt} \tag{7}$$

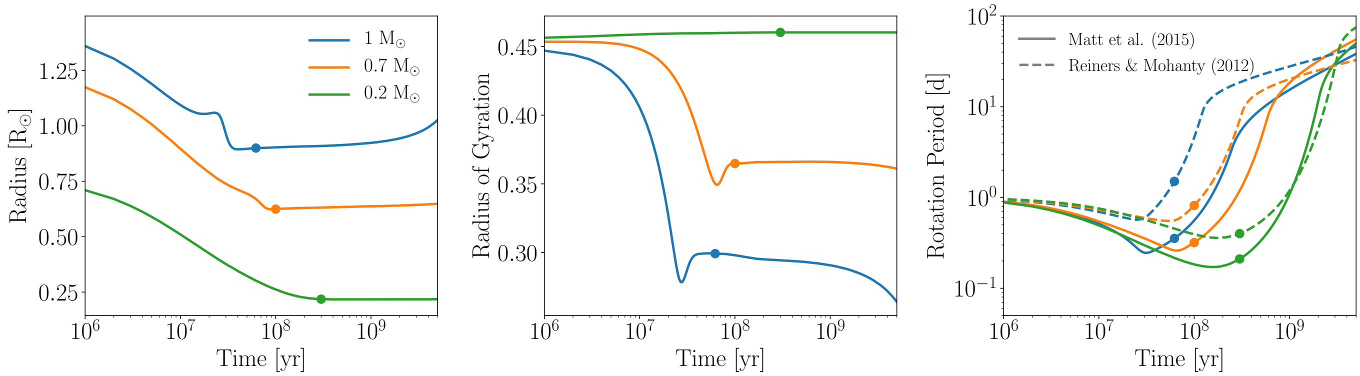

Figure 1. Stellar R (left), r_g (middle), and P_{rot} (right) evolution for 0.2 $M_\odot$ (M, green), 0.7 $M_\odot$ (K, orange), and 1 $M_\odot$ (G, blue) mass stars computed according to STELLAR, our interpolation of the Baraffe et al. (2015) stellar evolution models (§ 2.1) combined with the Matt et al. (2015) (solid) and Reiners & Mohanty (2012) (dashed) magnetic braking equations. Each dot denotes the approximate time when each star reaches the main sequence.

where if the i^{th} body is tidally-locked in a synchronous orbit,

$$\frac{da_{i,sync}}{dt} = -\frac{a^2}{Gm_1m_2}Z_{i,\mathrm{CPL}}\left(7e^2+\sin^2(\psi_i)\right)\varepsilon_{2,i}, \quad (8)$$

otherwise

$$\frac{da_i}{dt} = \frac{a^2}{4Gm_1m_2}Z_{i,\mathrm{CPL}}\left(4\varepsilon_{0,i}+e^2\left[-20\varepsilon_{0,i}+\frac{147}{2}\varepsilon_{1,i} + \frac{1}{2}\varepsilon_{2,i}-3\varepsilon_{5,i}\right]-4\sin^2(\psi_i)\left[\varepsilon_{0,i}-\varepsilon_{8,i}\right]\right). \quad (9)$$

The CPL equations for ψ and ω evolution are

$$\frac{d\psi_i}{dt} = \frac{Z_{i,\mathrm{CPL}}\sin(\psi_i)}{4m_ir_{g,i}^2R_i^2n\omega_i}\left([1-\xi_i]\varepsilon_{0,i}+[1+\xi_i](\varepsilon_{8,i}-\varepsilon_{9,i})\right) \quad (10)$$

$$\frac{d\omega_i}{dt} = -\frac{Z_{i,\mathrm{CPL}}}{8m_ir_{g,i}^2R_i^2n}\left(4\varepsilon_{0,i}+e^2\left[-20\varepsilon_{0,i}+49\varepsilon_{1,i}+\varepsilon_{2,i}\right] +2\sin^2(\psi_i)\left[-2\varepsilon_{0,i}+\varepsilon_{8,i}+\varepsilon_{9,i}\right]\right) \quad (11)$$

where G is Newton's gravitational constant, n is the binary's mean motion, and the index i denotes that i^{th} body. The tidal phase lags signs, ε, for the i^{th} body are given by

$$\begin{aligned}
\varepsilon_{0,i} &= \Sigma(2\omega_i-2n)\\
\varepsilon_{1,i} &= \Sigma(2\omega_i-3n)\\
\varepsilon_{2,i} &= \Sigma(2\omega_i-n)\\
\varepsilon_{5,i} &= \Sigma(n)\\
\varepsilon_{8,i} &= \Sigma(\omega_i-2n)\\
\varepsilon_{9,i} &= \Sigma(\omega_i)
\end{aligned} \quad (12)$$

where the function $\Sigma(x)$ returns 1 for positive x, -1 for negative x, and 0 otherwise.

The intermediate variable $Z_{\mathrm{CPL},i}$ is given by

$$Z_{i,\mathrm{CPL}} = 3G^2k_{2,i}M_j^2(M_i+M_j)\frac{R_i^5}{a^9}\frac{1}{nQ_i} \quad (13)$$

where the j^{th} body is the i^{th} body's companion, k_2 is the body's Love number of degree 2, and Q is the tidal quality factor ("tidal Q"). The tidal Q parameterizes the energy dissipation due to tidal evolution, with lower tidal Qs, i.e. larger phase differences between the tidal bulges, driving more rapid tidal evolution.

The other intermediate variable, ξ_i, is defined as

$$\xi_i = \frac{r_{\mathrm{g},i}^2R_i^2\omega_ian}{GM_j}. \quad (14)$$

2.2.2. *Constant Time Lag Model*

The "Constant Time Lag" (CTL) (Hut 1981; Leconte et al. 2010) equilibrium tidal model assumes a constant time interval between the body's tidal bulge and the passage of the tidally-interacting companion. In this formalism, unlike the CPL model, the CTL model is continuous over a range of tidal wave frequencies and applicable for large e. However if the assumption of linearity is relaxed, i.e. frequencies associated with tidal bulges are allowed to depend on a spin or orbital forcing frequency, then this model is only valid over a small range of frequencies (Greenberg 2009). We use the EQTIDE implementation of the CTL model in VPLanet following the derivation of Leconte et al. (2010). The equations that govern the secular changes in e, a, ω, and ψ are as follows:

$$\frac{de}{dt} = \frac{11ae}{2GM_1M_2}\sum_{i=1}^{2}Z_{\mathrm{CTL},i}\left(\cos(\psi_i)\frac{f_4(e)}{\beta^{10}(e)}\frac{\omega_i}{n}-\frac{18}{11}\frac{f_3(e)}{\beta^{13}(e)}\right), \quad (15)$$

$$\frac{da}{dt} = \frac{2a^2}{GM_1M_2}\sum_{i=1}^{2} Z_{\mathrm{CTL},i}\left(\cos(\psi_i)\frac{f_2(e)}{\beta^{12}(e)}\frac{\omega_i}{n} - \frac{f_1(e)}{\beta^{15}(e)}\right), \tag{16}$$

$$\frac{d\omega_i}{dt} = \frac{Z_{\mathrm{CTL},i}}{2M_i r_{g,i}^2 R_i^2 n}\left(2\cos(\psi_i)\frac{f_2(e)}{\beta^{12}(e)} - \left[1+\cos^2(\psi)\right]\frac{f_5(e)}{\beta^9(e)}\frac{\omega_i}{n}\right), \tag{17}$$

and

$$\frac{d\psi_i}{dt} = \frac{Z_{\mathrm{CTL},i}\sin(\psi_i)}{2M_i r_{g,i}^2 R_i^2 n\omega_i}\left(\left[\cos(\psi_i) - \frac{\xi_i}{\beta}\right]\frac{f_5(e)}{\beta^9(e)}\frac{\omega_i}{n} - 2\frac{f_2(e)}{\beta^{12}(e)}\right). \tag{18}$$

where the intermediate variables are given by

$$Z_{i,\mathrm{CTL}} = 3G^2 k_{2,i} M_j^2 (M_i + M_j)\frac{R_i^5}{a^9}\tau_i, \tag{19}$$

and

$$\begin{aligned}
&\beta(e) = \sqrt{1-e^2},\\
&f_1(e) = 1 + \tfrac{31}{2}e^2 + \tfrac{255}{8}e^4 + \tfrac{185}{16}e^6 + \tfrac{25}{64}e^8,\\
&f_2(e) = 1 + \tfrac{15}{2}e^2 + \tfrac{45}{8}e^4 + \tfrac{5}{16}e^6,\\
&f_3(e) = 1 + \tfrac{15}{4}e^2 + \tfrac{15}{8}e^4 + \tfrac{5}{64}e^6,\\
&f_4(e) = 1 + \tfrac{3}{2}e^2 + \tfrac{1}{8}e^4,\\
&f_5(e) = 1 + 3e^2 + \tfrac{3}{8}e^4.
\end{aligned} \tag{20}$$

In both the CPL and CTL model, We assume $k_2 = 0.5$. This choice of k_2 does not impact our results as k_2 is degenerate with Q in the CPL model, e.g. the k_2/Q scaling in Eq. (13), and with τ in the CTL model, e.g. $k_2\tau$ scaling in Eq. (19), so we instead examine how our results scale with Q and τ. Any constraints we derive as a function Q or τ can trivially be scaled to other values of k_2.

2.2.3. *Tidal Locking*

Tidal torques drive a body's rotation rate towards the tidally-locked state. When a body tidally locks, tidal torques fix P_{rot} to the equilibrium P_{rot}, P_{eq}. Typically, tidal locking is understood in the context of a synchronized rotator, e.g. when $P_{rot} = P_{eq} = P_{orb}$. Although spin-orbit synchronization is an expected outcome of tidal evolution (Counselman 1973), in general for tidally-locked bodies on non-circular orbits, both the CPL and CTL model predict pseudosynchronous, or supersynchronous rotation, e.g. Mercury's 3:2 spin-orbit resonance ($P_{rot} = 2/3\ P_{orb}$, Goldreich & Peale 1966).

The CPL model, owing to its assumption of a finite number of discrete tidal lags, only permits a 1:1 and 3:2 spin-orbit state where, following Barnes (2017), the CPL P_{eq} is given by

$$P_{eq}^{\mathrm{CPL}} = \begin{cases} P_{orb} & \text{if } e < \sqrt{1/19} \\ \frac{2}{3}P_{orb} & \text{if } e \geq \sqrt{1/19}. \end{cases} \tag{21}$$

Therefore, the CPL model predicts synchronous rotation for $e \lesssim 0.23$, and a supersychronous 3:2 spin-orbit state otherwise for tidally-locked rotators.

We note that two discrete rotation states are not the only permitted ones for tidally-locked systems under the CPL formalism. For example, an alternate derivation of P_{eq} for orbiters with rotation axes perpendicular to the orbital plane under the CPL model predicts

$$P_{eq} = \frac{P_{orb}}{1+9.5e^2}, \tag{22}$$

a continous function of e (Goldreich 1966; Murray & Dermott 1999). Here, we follow the suggestions of both Barnes et al. (2013) and Barnes (2017) and use the discrete P_{eq} version of the CPL model for self-consistency.

The CTL model is continuous over a range of tidal frequencies and therefore predicts a P_{eq} that is a continuous function of both e and ψ. Following Barnes (2017), we define the CTL P_{eq} by

$$P_{eq}^{\mathrm{CTL}} = P_{orb}\frac{\beta^3 f_5(e)(1+\cos^2(\psi))}{2f_2(e)\cos(\psi)}. \tag{23}$$

The CTL model predicts that bodies on eccentric orbits tidally-lock into supersyncronous rotation, and only bodies with aligned spins on circular orbits are synchronous rotators.

In general, a continuous P_{eq} and the discrete 1:1 and 3:2 spin-orbit commensurabilities are not the only equilibrium rotation states for tidally-locked rotators predicted by equilibrium tidal models. For example, Rodríguez et al. (2012) show that tidally-interacting bodies can get captured into many spin-orbit resonances states, e.g. 2:1, 5:2, 4:3, etc. Although our models do not resolve capture into such states, we search for evidence of them in data of the spin-orbital states *Kepler* EBs.

2.2.4. *Numerical Details of Tidal Locking*

Due to the discontinuities in the equilibrium tidal model equations, for example in Eq. (12) when $\omega \approx n$, and due to the inherant discreteness of numerical integrations, numerical solutions for the CPL and CTL models can produce unphysical evolution. We follow Barnes et al. (2013) and Fleming et al. (2018) and fix $P_{rot} = P_{eq}$ according to Eq. (21) or Eq. (23) for the CPL and CTL models, respectively, when P_{rot} is within 1% of P_{eq}. To ensure that tidal torques dominate over torques due to magnetic braking and stellar evolution when forcing tidal-locking, we additionally require that the P_{rot} derivative points towards P_{eq} on both sides of P_{eq}, i.e. when the gradient of P_{rot} points towards the tidally-locked state, before fixing $P_{rot} = P_{eq}$. We find that this scheme produces physically and numerically accurate results.

2.2.5. *Example Tidal Evolution*

We plot the tidal evolution for a, e, and ω, ignoring stellar evolution, for a solar-twin binary with an initial $P_{orb} = 10$ d, $P_{rot} = 1$ d, $e = 0.2$ for the CPL model and CTL model, assuming $Q = 10^6$ and $\tau = 0.1$ seconds, respectively, in Fig. 2. Both the CPL and CTL model predict the same qualitative evolution: both the binary's e and P_{orb} slightly increase as tides force the spins toward the tidally-locked state, transferring rotational angular momentum into the orbit in the process. At late times, both the CPL and CTL drive the binaries towards orbital circularization, with tidal dissipation decreasing P_{orb}. The predictions of the CPL and CTL model, differ, however, when the binaries tidally-lock. Under the CPL model, the binary tidally-locks into a synchronous orbit when $e < \sqrt{1/19}$, e.g. Eq. (21), while the CTL model predicts supersyncronous rotation due to the CTL model's equilibrium period eccentricity dependence, e.g. Eq. (23).

2.3. *Coupled Stellar-Tidal Evolution For Tidally-Locked Systems*

Following Fleming et al. (2018), when one or both binary stars are tidally locked, tidal forces prevent magnetic braking from spinning down the tidally-locked star(s), and any angular momentum lost comes at the expense of the binary orbit, decreasing a as a result (Verbunt & Zwaan 1981). Below in Eq. (24) and Eq. (25), we modify the a decay equations due to stellar evolution and magnetic braking in tidally-locked binaries from Fleming et al. (2018), their Eqs. (18) and (20), to additionally account for r_g evolution when one or both stars tidally-lock, respectively, assuming conservation of angular momentum:

$$\dot{a}^{(1)}_{coupled} = \frac{-\dot{J}_{mb} - 2\omega\left(m_1 r_{g,1}^2 R_1 \dot{R}_1 - m_1 r_{g,1}\dot{r}_{g,1} R_1^2\right)}{\frac{\mu^2 GM(1-e^2)}{2J_{orb}} - \frac{3\omega}{2a} m_1 r_{g,1}^2 R_1^2} \quad (24)$$

and

$$\dot{a}^{(2)}_{coupled} = \frac{-\dot{J}_{mb} - 2\omega\left(\sum_{i=1}^{2} m_i r_{g,i}^2 R_i \dot{R}_i + m_i r_{g,i}\dot{r}_{g,i} R_i^2\right)}{\frac{\mu^2 GM(1-e^2)}{2J_{orb}} - \frac{3\omega}{2a}\left(m_1 r_{g,1}^2 R_1^2 + m_2 r_{g,2}^2 R_2^2\right)} \quad (25)$$

where J_{orb} is the orbital angular momentum.

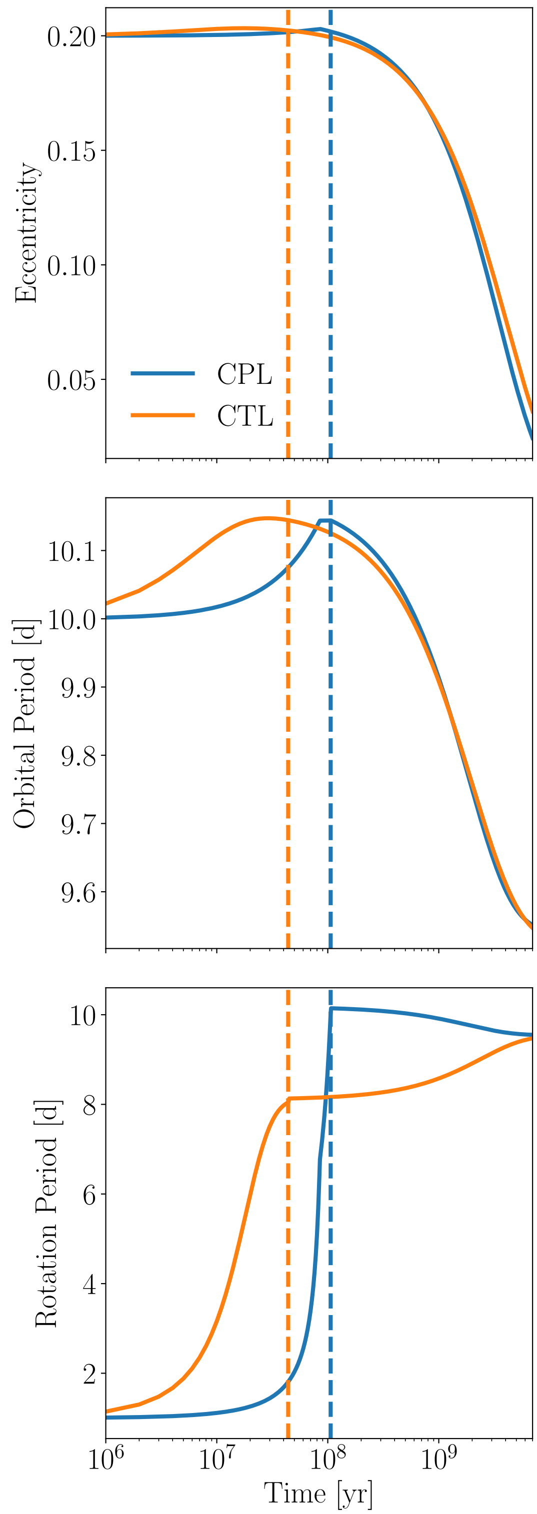

Figure 2. Tidal evolution of a 1 $M_\odot$− 1 $M_\odot$ stellar binary's e (top), P_{orb} (middle) and P_{rot} (bottom) for the CPL (blue) and CTL (orange) model. The blue (CPL) and orange (CTL) vertical dashed lines denote when the stellar binary tidally locks. Both the CPL and CTL model predict the same qualitative evolution. The rotational evolution differs, however, as under the CPL model, the binary tidally-locks into a synchronous orbit as $e < \sqrt{1/19}$, e.g. Eq. (21), while the CTL model predicts supersyncronous rotation due to the CTL model's equilibrium period eccentricity dependence (see Eq. (23)).

3. SIMULATIONS

We examine stellar angular momentum evolution in low-mass binaries by simulating four sets of 10,000 stellar binaries, one modeled using the CPL model and the other using the CTL formalism, using both magnetic braking models. We simulate both stars' spin evolution but mainly consider the P_{rot} evolution for the primary, i.e. more massive star in binaries, as it is observationally easier to measure a P_{rot} on the more massive, and hence brighter, star (e.g. Meibom et al. 2006; Lurie et al. 2017). For each simulation, we sample the primary's mass uniformly over $[0.1, 1]$ $M_{\odot}$. Following Matt et al. (2015), we uniformly sample the $\log_{10}$ of P_{rot} over $[0.8, 15]$ days, a distribution that approximates the P_{rot} distribution of young stars in the ∼2 Myr old Orion Nebula Cluster (Stassun et al. 1999; Herbst et al. 2001, 2002; Rodríguez-Ledesma et al. 2009). We compute the secondary star's mass by uniformly sampling the mass ratio over $[0.1, 1]$ following observations of mass ratios in low-mass binaries (Raghavan et al. 2010; Moe & Kratter 2018). Given the inherent uncertainty in and complexity of the formation of short-period binaries (e.g. Bonnell & Bate 1994; Bate 2000; Bate et al. 2002; Moe & Kratter 2018) and the potential for dynamical processing via tides or stellar close encounters (e.g. Mardling & Aarseth 2001; Hurley et al. 2002; Ivanova et al. 2005; Meibom & Mathieu 2005), we take an agnostic approach to the initial orbital configuration by uniformly randomly sampling the initial eccentricity (e) over $[0.0, 0.3]$, consistent with eccentricities of field binaries that likely have not been tidally-processed (Raghavan et al. 2010). Although the CTL model is applicable for $e \gtrsim 0.3$, the CPL model is not, so we restrict $e \leq 0.3$ to allow us to compare both models. We uniformly sample the initial P_{orb} over $[3, 100]$ d and do not consider $P_{orb} < 3$ d as these binaries are likely to have a tertiary companion (Tokovinin et al. 2006) which can significantly impact the inner binary's dynamical evolution (e.g. Muñoz & Lai 2015; Martin et al. 2015; Hamers et al. 2016; Moe & Kratter 2018).

Values for stellar tidal Qs and τs for low-mass stars are highly uncertain due to complex viscous evolution within the stars (Ogilvie & Lin 2007), and can differ for stars of the same spectral class (Barker & Ogilvie 2009). These parameters can also vary as a function of stellar mass or age (Bolmont & Mathis 2016; Van Eylen et al. 2016), likely due to low-mass stars' evolving convective regions where the tidal dissipation predominantly occurs (Zahn 2008). Typical values of Q and τ for Sun-like stars are estimated to be of order $Q \approx 10^6$ and $\tau \approx 0.1$ s, respectfully (e.g. Meibom & Mathieu 2005; Ogilvie & Lin 2007; Jackson et al. 2008), however a range of values exist in the literature. Therefore, we consider a wide range of tidal parameters by sampling stellar tidal Qs log-uniformly over $[10^4, 10^8]$ and τ log-uniformly over $[10^{-2}, 10]$ s. There is no general expression to compute Q as a function of τ, or vice versa, except in some special cases where approximations exist, e.g. Eqn. (2) from Heller et al. (2011).

We explore the impact of both the Matt et al. (2015) and Reiners & Mohanty (2012) magnetic braking models, but default to using the Matt et al. (2015) unless noted otherwise. All stars have an initial age of 5 Myr unless stated otherwise as by this time, the gaseous protoplanterary circumbinary disk that can drive significant dynamical evolution in the binary (e.g. Fleming & Quinn 2017) would likely have dissipated (Haisch et al. 2001).

We also perform a smaller subset of simulations to illustrate the behaviour of our coupled model and describe their initial conditions as we introduce them. All code used to run simulations and generate figures is available online[2].

4. RESULTS

4.1. *Interaction Between Magnetic and Tidal Braking: Subsynchronous Rotation*

Here we focus on binaries in weak tides regime, i.e. long P_{orb} and large Q or small τ, to identify the boundary between evolution dominated by tides or magnetic braking via analytic calculations and simulations.

4.1.1. *Analytic Torque Balance*

In the weak tides regime, spin-down due to magnetic braking will drive the stellar P_{rot} past P_{eq}, resulting in subsynchronous rotation. In this case when $P_{rot} > P_{eq}$ for long P_{orb}, the stars will be slowly-rotating and in the unsaturated magnetic braking regime (Matt et al. 2015). Since magnetic braking scales as P_{rot}^{-3} for unsaturated rotators, e.g. Eqn. (2), magnetic braking torques weaken as the stellar rotation slows down, so at some P_{rot}, tidal torques that try to spin-up subsynchronous rotators back towards P_{eq} will balance the spin-down torque of magnetic braking, producing a long-lasting state of subsynchronous rotation.

We compute the P_{rot} at which this balance occurs by by setting the sum of Eqn. (17) and Eqn. (2) equal to 0, noting that $d\omega/dt = (1/\mathrm{I})dJ/dt$ for fixed moment of inertia, I. In this calculation, we consider tidal torques under the CTL formalism and magnetic braking under the Matt et al. (2015) model. For simplicity, we assume both stars are solar-mass with 0 obliquity, a circular binary

[2] https://github.com/dflemin3/sync.

orbit, and that the torque balance occurs while the stars are on the main sequence where stellar properties change slowly, allowing us to set $R = 1R_\odot$ and assume constant moments of inertia. We find below in simulations that these assumptions are well-justified. Given these assumptions, we can specify P_{orb}, k_2, and τ to compute the equilibrium P_{rot} at which tidal and magnetic braking torques balance. We derive this balance, given by Eqn. A4, in § A and visualize it in Fig. 3. We normalize P_{rot} by P_{eq}, which for binary stars with 0 obliquity on circular orbits is simply P_{orb} (see Eqn. (23)).

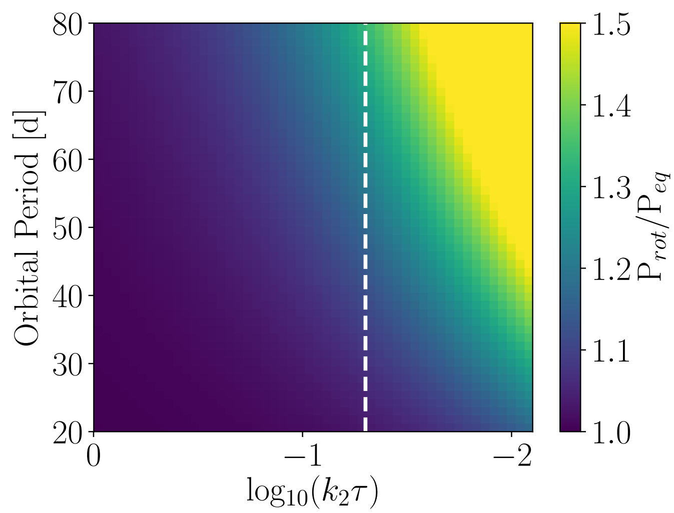

Figure 3. The stellar P_{rot}, normalized by P_{eq}, at which the torques due to magnetic braking and tides balance for a 1 $M_\odot - 1\ M_\odot$ binary on a circular orbit according to Eqn. A4. The white dashed line indicates our fiducial values for k_2 and τ, 0.5 and 0.1 s, respectively, that we adopt in the simulations in § 4.1.2.

In general as tides weaken, i.e. increasing P_{orb} and/or decreasing $k_2\tau$, tidal and magnetic braking torques balance at longer P_{rot} where magnetic braking torques are weaker, or equivalently at larger P_{rot}/P_{eq}. Conversely, in the strong tides regime, $k_2\tau \gtrsim -1$, tidal torques overpower magnetic braking for most orbital periods, tidally-locking binaries into synchronous rotation. Given this calculation, we expect that for many orbital periods and tidal time lags, stellar binaries will reach a state of subsynchronous rotation. For our fiducial values of $k_2 = 0.5$ and $\tau = 0.1$ s (white dashed line in Fig. 3), solar-twin binaries on low eccentricity orbits reach the subsynchronous state with $P_{rot}/P_{eq} \approx 1.1 - 1.4$, with this value increasing with P_{orb}. This simple analytic calculation, however, does not account for stellar evolution or secular orbital evolution due to tides, e.g. tidal friction that will shrink the orbit, gradually strengthening tidal torques, so we cannot precisely determine when the binaries reach the subsynchronous state nor how long it will last. For that, we turn to simulations.

Below, we verify the results of our analytic calculations by examining how stellar binaries evolve towards subsynchronous rotation, under what conditions, and when it occurs in the weak tides regime. We simulate the full coupled stellar-tidal evolution of $1\ M_\odot - 1\ M_\odot$ binaries on initially circular orbits with a combination of both tidal models and both magnetic braking models. In Fig. 4, we plot the simulated evolution of P_{rot}, normalized by P_{eq}, and its time derivative for $P_{orb} \in [5, 60]$ d modeled using both the CPL (solid line, $Q = 10^6$) and CTL (dashed line, $\tau = 0.1$ s) models.

4.1.2. *Torque Balance Using the Matt et al. (2015) Magnetic Braking Model*

Both tidal models predict that binaries with $P_{orb} < 10$ d will tidally-lock within 100 Myr, in agreement with observations (Meibom & Mathieu 2005) and previous theoretical work (Zahn & Bouchet 1989). The CPL model predicts that each binary tidally-locks, even out to $P_{orb} = 60$ d, indicating that tidal locking is not necessarily restricted to short P_{orb} systems. The CTL model, however, predicts that for $P_{orb} \gtrsim$10 d, magnetic braking overpowers weak tidal torques, spinning down the stars past the tidally-locked state. Magnetic braking pushes $P_{rot}/P_{eq} \approx 1.1$ with the maximum value set by the torque balance between tidal torques and magnetic braking, in good agreement with the analytic calculations in § 4.1.1. As shown in § 4.1.1, the peak P_{rot}/P_{eq} grows for longer P_{orb} since tides weaken with increasing binary separation, e.g. Eqn. (19), allowing magnetic braking to dominate the spin evolution, driving the binaries towards subsynchronous rotation.

Subsynchronous rotation does not persist indefinitely, however, as P_{rot} eventually decreases back towards the tidally-locked state in the long-term due to a combination of three simultaneous physical effects. First, as P_{rot} continue to increase due to magnetic braking, magnetic braking itself weakens as its torque scales as P_{rot}^{-3} for unsaturated rotators (Matt et al. 2015). Second, as P_{rot} increases further from the tidally-locked state, tidal torques strengthen as they try to force P_{rot} back towards P_{eq} (see Eqn. (17), for example). Third, when $P_{rot} > P_{eq}$, tides transfer angular momentum from the orbit into stellar rotations, decreasing P_{orb} and strengthening tidal torques that strongly depend on the binary separation as $a^{-6.5}$. These effects combine to shift the balance of power from magnetic braking-controlled stellar spin down to tidal torques spinning-up stars, shepherding them towards P_{eq} in the long term.

We can see this process unfold in the right panel of Fig. 4 where we plot the total P_{rot} time derivative due

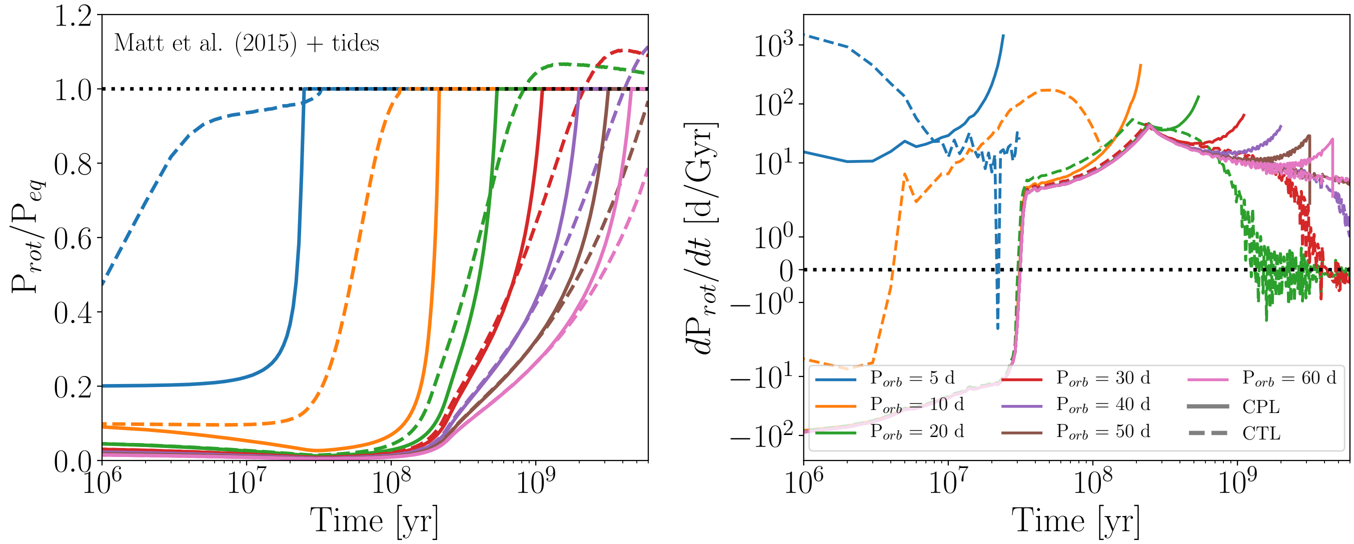

Figure 4. Evolution of stellar P_{rot}, normalized by P_{eq} (see Eqn. (21) and Eqn. (23), for initial circular binary orbits according to the CPL (solid) and CTL (dashed) models with $Q = 10^6$ and $\tau = 0.1$ s, respectively, using the Matt et al. (2015) magnetic braking model. Left: P_{rot}/P_{eq} for stars with P_{orb} ranging from 5 d to 60 d. The black dotted line indicates the tidally-locked state where $P_{rot} = P_{eq}$. Right: Net P_{rot} derivative due to stellar evolution, tidal torques, and magnetic braking. We truncate each curve when the binary tidally locks. For $P_{orb} \leq 10$ d, both the CPL and CTL models predict that the binaries lock into synchronous rotation. For all P_{orb}, the CPL models tidally-lock into synchronous rotation whereas the CTL model predicts subsynchronous ($P_{rot} > P_{eq}$) rotation that persists for Gyrs.

to stellar evolution, magnetic braking, and tidal torques as a function of time in our simulations. Early on, $\dot{P}_{rot} < 0$ as stars contract along the pre-main sequence until about 60 Myr when the stars reach the main sequence. After R contraction, $\dot{P}_{rot} > 0$ as tides and magnetic braking combine to spin down stars towards the tidally-locked state. For the CTL models with $P_{orb} > 10$ d, $\dot{P}_{rot} > 0$ driving the stars towards subsynchronous rotation. $\ddot{P}_{rot} < 0$, however, as the three processes described above gradually strengthen tidal torques relative to magnetic braking. In the long-run, tidal torques overpower magnetic braking, with a slightly negative P_{rot} derivative, slowly driving P_{rot} back towards P_{eq} (see the $P_{orb} = 20, 40$ d cases in Fig. 4). This slowly shifting torque balance produces a population of subsynchronous rotators with $P_{rot} > P_{eq}$ that can persist for Gyrs.

4.1.3. *Torque Balance Using the Reiners & Mohanty (2012) Magnetic Braking Model*

The mechanism for producing subsynchronous rotation is not limited to the Matt et al. (2015) magnetic braking model, but is a generic outcome of the coupling of magnetic braking and weak tidal torques. The CTL model can only tidally-lock the $P_{orb} = 5$ d binary as the stronger magnetic braking under the Reiners & Mohanty (2012) model forces the longer P_{orb} binaries into subsynchronous rotation. Curiously, all CTL subsynchronous rotators seem to converge to $P_{rot}/P_{eq} \approx 1.1$. In this state, tidal torques nearly balance magnetic braking, producing a long-lasting population of subsynchronous rotators, similar to what was observed above. In the right panel of Fig. 5, we see that the net P_{rot} derivatives for these binaries oscillate about 0, but are slightly negative due to the 3 simultaneous physical effects described above. This slight negative derivative is effectively negligible, however, as the torque balance will likely hold the binaries in subsynchronous rotation for 10s of Gyrs. We note that in other exploratory simulations with larger τ, we find that the tides do in fact eventually win out over magnetic braking in the long-run, driving P_{rot} back towards P_{eq}.

4.1.4. *Subsynchronous Rotation at Short P_{orb}*

In Fig. 6, we examine subsynchronous rotation in short P_{orb} binaries by displaying the P_{rot} evolution for a $P_{orb} = 5$ d binary for various tidal dissipation parameters. Subsynchronous rotation occurs in general for weak tidal torques, $Q > 10^7$ or $\tau < 0.1$ s in these cases, and is not restricted to long P_{orb} binaries. Previous theoretical studies have also predicted subsynchronous rotation in short P_{orb} binaries arising from the balance between tidal torques and magnetic braking (e.g. Habets & Zwaan 1989; Zahn 1994; Keppens 1997) suggesting that this behavior is not an artifact of our choice of tidal or magnetic braking models, but rather a general outcome of the competition between magnetic braking and tidal evolution in low-mass binaries. Short P_{orb} subsynchronous rotators can eventually tidally-lock via the

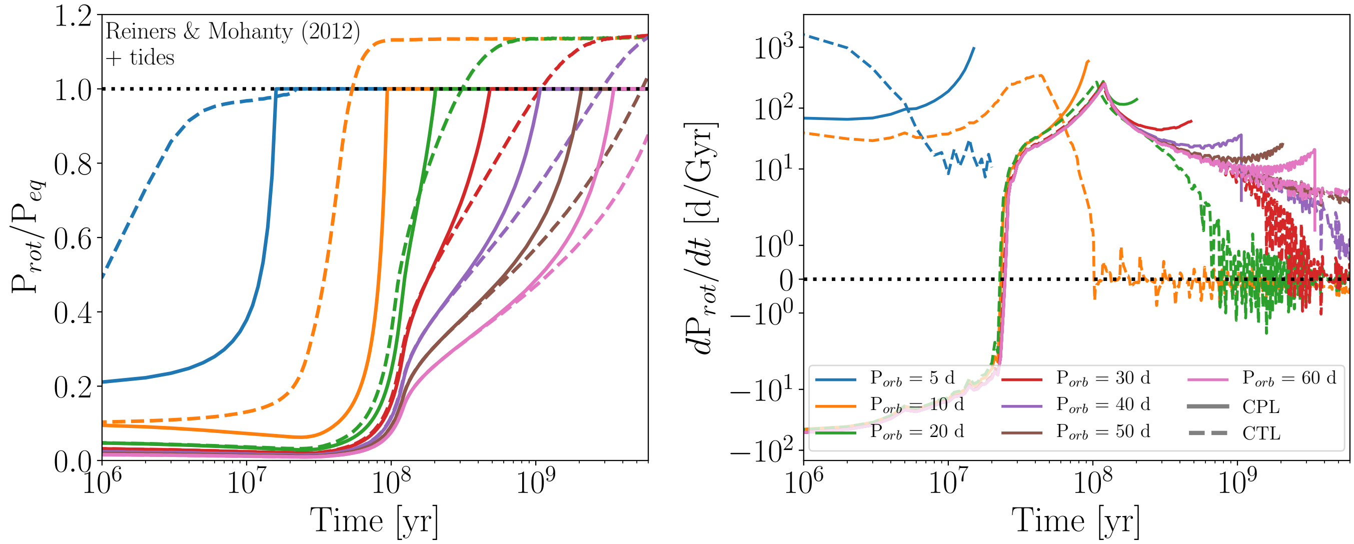

Figure 5. Same format as Fig. 4, but evolved using the Reiners & Mohanty (2012) magnetic braking model.

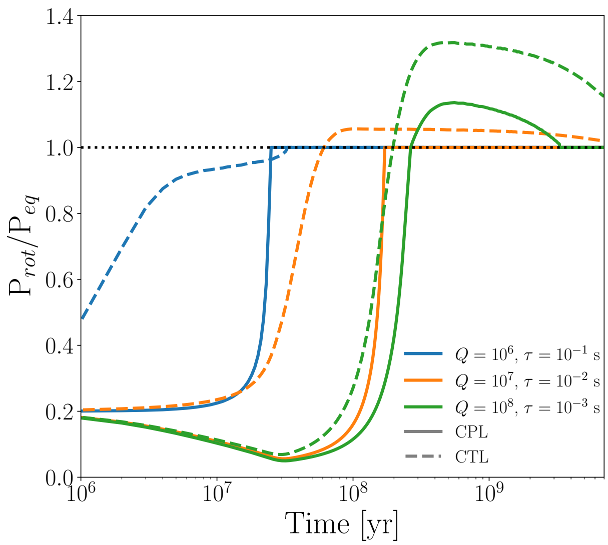

Figure 6. Evolution of stellar P_{rot}, normalized by P_{eq} (see Eqn. (21) and Eqn. (23), for initial circular binary orbits with initial P_{orb} = 5 d according to the CPL (solid) and CTL (dashed) models for several values of Q and τ, respectively, using the Matt et al. (2015) magnetic braking model. Systems with strong tidal torques ($Q = 10^6$ or $\tau = 0.1$ s) tidally lock, whereas in systems with weaker tidal torques (larger Q and smaller τ, respectively), magnetic braking initially overpowers tidal torques, spinning down the stars past the tidally-locked state, resulting in subsynchronous rotation.

mechanism described above where tidal torques gradually strengthen relative to magnetic braking.

Short P_{orb} subsynchronous binaries exist in nature, such as many *Kepler* EBs (Lurie et al. (2017), see § 4.5 for further discussion), Kepler-47 (Orosz et al. 2012), EPIC 219394517 (Torres et al. 2018), and in "Binary 6211" observed by Meibom et al. (2006), suggesting that this theoretical observation is real and borne out in nature. Spin-orbit synchronization should therefore not be assumed for short P_{orb} binaries and sunsynchronous rotation should be expected in many tidally-interacting binaries. We explore these effect further and compare our theory to observations of *Kepler* EBs in § 4.5.

4.2. *Influence of P_{orb}, Q and τ*

We next examine how P_{rot} evolution in stellar binaries depends on P_{orb} and the strength of tidal dissipation, parameterized by Q and τ for the CPL and CTL models, respectfully. In Fig. 7, we bin our simulation results after the full 7 Gyr evolution by P_{orb} and Q or τ and compute the median P_{orb}/P_{rot} in each bin, marginalizing over all other parameters.

Spin-orbit synchronization is the typical outcome for binaries with $P_{orb} < 10$ d according to the CPL model for most values of Q. The strong tidal torques predicted by the CPL model can even tidally-lock binaries out to $P_{orb} \approx 100$ d for $Q < 10^5$, well beyond the expected limit of 20 d (Meibom et al. 2006). According to the CTL model, binaries with $P_{orb} < 10$ d typically tidally-lock for $\tau \gtrsim 0.1$ s, and seldomly tidally-lock for $P_{orb} > 20$ d, except for systems with strong tides, $\tau \gtrsim 3$ s. Both models predict a substantial population of subsynchronous rotators (red regions in Fig. 7, $P_{rot} > P_{orb}$), consistent with magnetic braking dominating weak tidal torques, i.e. stars with large Q or small τ, that form via the mechanism described in § 4.1, with weaker tidal torques allowing more subsynchronous rotation. The population of supersynchronous rotators (blue regions in Fig. 7, $P_{rot} < P_{orb}$) with $P_{orb} > 80$ d does not in general correspond to binaries tidally-locking into supersynchronous rotation, but rather, typically arises from the combination of weak tidal torques and magnetic braking not spinning down stars enough for P_{rot} to be close to the tidally-locked state.

Both tidal models predict a population of nearly synchronous rotators near $P_{orb} \approx 60$ d. This population corresponds to the evolution described in § 4.1 in which magnetic braking initially spins down stars past the tidally-locked state, but in the long-term, tidal torques spin up the stars, shepherding them towards the tidally-locked state. This process can keep stellar $P_{rot} \gtrsim P_{eq}$ for several Gyrs or longer, depending on the P_{orb} and Q or τ (see Figs. 4,6).

We isolate the impact of Q and τ by binning our simulation results after 7 Gyr of evolution by P_{orb} and P_{orb}/P_{rot}. In each bin, we compute the median Q and τ, and the 16%, and 84% percentiles, a measure of the spread of the distribution, to quantify the distribution of tidal strength parameters that are consistent with each spin-orbital state.

For all P_{orb} in Fig. 8, synchronous and supersynchronous rotators have systematically low Qs, typically $Q < 10^6$, as strong tidal torques are required to tidally-lock the systems, especially for $P_{orb} > 20$ d. For $P_{orb} <$ 10 d, there are no rotators with $1.0 < P_{orb}/P_{rot} < 1.5$ nor do any stars have $P_{orb}/P_{rot} > 1.5$ for $P_{orb} < 70$ d as in the CPL model, binaries with eccentric orbits can only tidally-lock into a 1:1 or 3:2 spin-orbit commensurability, i.e. Eqn. (21).

Subsynchronous rotators have systematically larger Qs, typically $Q > 10^6$, and hence experience weak tidal torques that are dominated by magnetic braking that spin-down the stars past the tidally-locked state. This effect can be seen for $P_{orb} < 50$ d where the median Q gradually increases with decreasing P_{orb}/P_{rot}, except near the tidally-locked state. This trend reverses at longer $P_{orb} > 60$ d where supersynchronous rotation arises from the inability of tidal torques and magnetic braking to spin-down stars enough to approach the tidally-locked state by the end of the simulation. In this case, the more supersynchronous the rotation, the weaker the tidal torques must be, and hence the larger the Q must be.

According to the CTL model, many binaries tidally-lock for $P_{orb} \lesssim$20 d. Tidally-locking can occur for $P_{orb} < 50$ d and $\tau \gtrsim$0.25 s. For $P_{orb} < 50$ d, subsynchronous rotation occurs for stars with $\tau < 0.1$ s as magnetic braking dominates over tidal torques. For $P_{orb} > 50$ d, magnetic braking dominates the evolution as the diagonal sequence with a median $\tau \approx 0.1$ s has upper and lower limits that encompass most of the range we considered for τ, suggesting that tides are not important in this region of parameter space. The shape of this diagonal region arises from the combination of magnetic braking and our flat initial P_{orb} distribution. We do not observe $P_{orb}/P_{rot} \gtrsim$1.5 as we only consider eccentricities up to $e = 0.3$, limiting how rapid supersynchronous systems can rotate according to Eqn. (23).

4.3. *P_{rot} Distribution of a Synthetic Population of Stellar Binaries*

Here we examine how the competition between tidal torques and magnetic braking shape the P_{rot} distribution of low-mass stellar binaries. We consider two cases where tidal torques dominate: "Locked" where $P_{rot} = P_{eq}$ and "Interacting" where P_{rot} is within 10% of P_{eq} as in this regime, tides are likely shepherding P_{rot} towards the tidally-locked state keeping P_{rot} close to P_{eq}, typically within about 10% as we demonstrated in § 4.1, e.g. Fig. 4. We refer to the remaining binaries as "Unlocked" as magnetic braking and stellar evolution likely dominate their angular momentum evolution. In Fig. 10 and Fig. 11, we plot P_{rot} as a function of mass for the primary stars in stellar binaries for both the CPL and CTL model, respectively, integrated to system ages uniformly sampled over $1 - 7$ Gyr.

Both models predict a substantial population of tidally-locked fast rotators with $P_{rot} \lesssim$20 d, with tidally-locked stars systematically rotating faster (median CPL, CTL $P_{rot} = 27.6$ d and 7.4 d) than unlocked (median CPL, CTL $P_{rot} = 41.3$ d and 40.8 d) binaries. More massive stars are more likely to tidally-lock compared to less massive stars as tidal torques scale as R^5, and R increases with stellar mass. This feature is seen in the enhanced density of locked systems at larger masses for both tidal models, but in particular for the CPL model.

Tidal locking is not limited to $P_{orb} \lesssim$20 d, however, as we find stellar binaries can tidally-lock over a wide range of P_{rot} up to $P_{rot} = P_{orb} \approx 100$ d according to the CPL model, producing a slow-rotating population above the P_{rot} distribution envelop of single stars. This behavior is consistent with observations of P_{rot} in *Kepler* eclipsing binaries by Lurie et al. (2017) who find tentative evidence that binaries can tidally-lock up to their detection limit of $P_{orb} = P_{rot} = 45$ d and with the observations of Abt & Boonyarak (2004). Under the CTL model, however, binaries predominantly tidally-lock out to only $P_{orb} \approx 20$ d, in stark contrast to the CPL model's predictions. Some binaries can tidally-lock or tidally-interact out to $P_{rot} \approx 80$ d, but not nearly as many as the CPL model, nor can the CTL model tidally-lock binaries out to $P_{orb} = 100$ d, regardless of τ. Only 7.5% of binaries tidally-lock according to the CTL model, compared with 25% of CPL model binaries, as tidal torques are generally stronger in the CPL formalism.

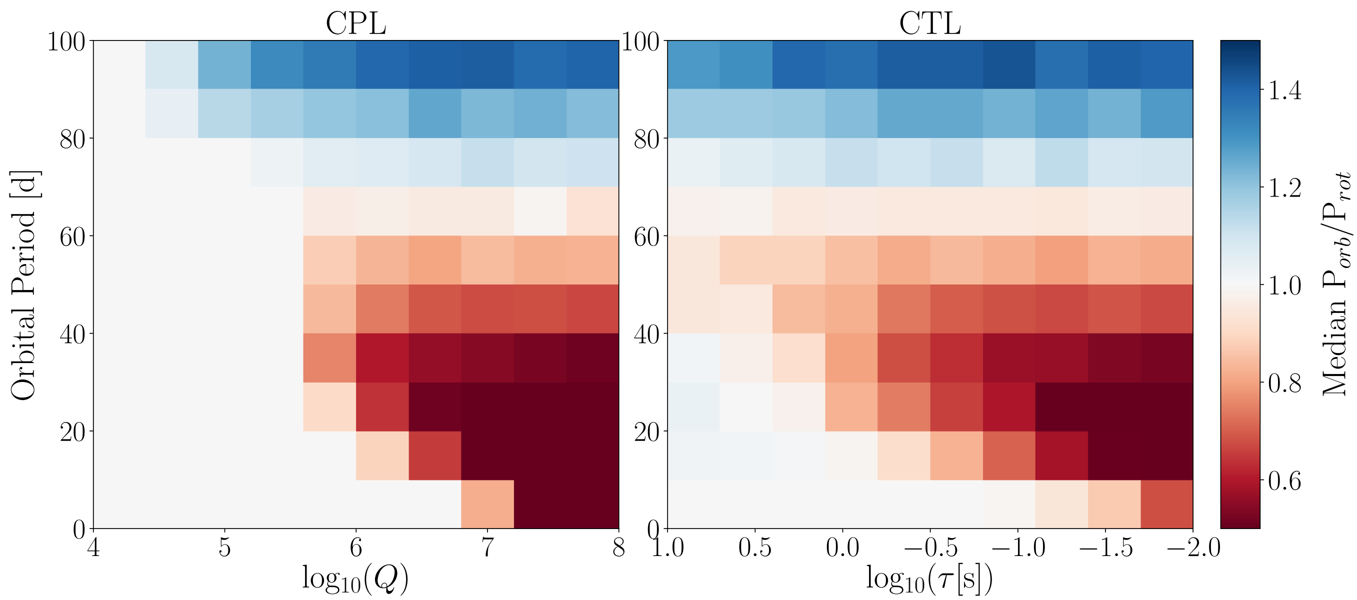

Figure 7. Median P_{orb}/P_{rot} at the end of the simulation according to the CPL (left) and CTL (right) models binned by $\log_{10}(Q)$ and $\log_{10}(\tau)$, respectively, and P_{orb}. For $P_{orb} < 10$ d, the CPL model predicts that most systems will tidally lock into synchronous rotation, regardless of Q, whereas the CTL model requires $\tau \geq 0.1$ s to tidally-lock. Both models exhibit supersynchronous rotation (blue regions, $P_{rot} < P_{orb}$) for $P_{orb} > 80$d, that do not in general reflect tidally-locking into a supersynchronous rotation, but rather at long P_{orb}, the combination of weak tidal torques and magnetic braking have not spun down the star enough for P_{rot} to be close to P_{orb} after 7 Gyr of evolution. For large Q ($> 10^{6.5}$) and small τ ($\tau < 0.1$ s), weak tidal torques cannot prevent magnetic braking from spinning down stars past the tidally-locked state, producing a population of subsynchronous rotators (red regions, $P_{rot} > P_{orb}$).

The interacting population tends to rotate more slowly than the unlocked population as at short P_{orb}, and hence P_{rot}, binaries preferentially tidally-lock due to stronger tidal torques. At longer P_{orb}, weaker tidal torques allow magnetic braking to spin down the stars past P_{eq}, with tidal torques eventually strengthening enough to shepherd P_{rot} towards P_{eq} via the mechanism discussed in § 4.1. The CPL and CTL models predict that 34% and 25% of stars, respectively, are either tidally-locked or interacting, demonstrating that tidal torques play a pivotal role in shaping the angular momentum evolution in stellar binaries across a wide range of parameters. The P_{rot} - mass distribution for unlocked binaries resembles the single star sequence observed in the center right panel of Fig. 13 indicating that magnetic braking and stellar evolution dictate their angular momentum evolution as expected.

As shown in Fig. 12, both models predict that tidal torques can influence the P_{rot} evolution out to $P_{orb} \approx 80$ d, causing a significant departure from the long-term expected spin down of single stars due to magnetic braking. The CTL model predicts that the majority tidally-locked binaries, 86%, lock into rapid rotation with $P_{rot} \lesssim 20$ d, typically in short P_{orb} binaries where tidal torques are strongest as the median locked CTL $P_{orb} = 7.6$ d. The CPL model, however predicts that binaries can tidally-lock into a wide range of rotation states with only 39% of locking binaries have $P_{rot} < 20$ d, while many lock out to $P_{rot} \approx 100$ d, with the latter state corresponding to tidal synchronization in long P_{orb} binaries. The presence of $P_{orb} > 20$ d locked population, or lack there of, could be a powerful observational discriminant between which equilibrium tidal model acts in low-mass stellar binaries. We discuss this point further in § 4.6.

4.4. *Deviations From Single Star P_{rot} Evolution: Implications for Gyrochronology*

We compare the P_{rot} distribution for tidally-interacting stellar binaries from our CPL and CTL simulations with the P_{rot} distribution of single stars subject to stellar evolution and magnetic braking to gauge the impact of tidal torques on driving P_{rot} distributions away from that of single stars. We simulate 10,000 single star systems according to the evolution described in § 2.1 with initial conditions sampled from the same mass and P_{rot} distributions used for the binary simulations described § 2. In Fig. 13, we display P_{rot} as a function of mass and age for binaries simulated using both the CPL and CTL model and for single stars. We perform this procedure for stars losing angular momentum via magnetic

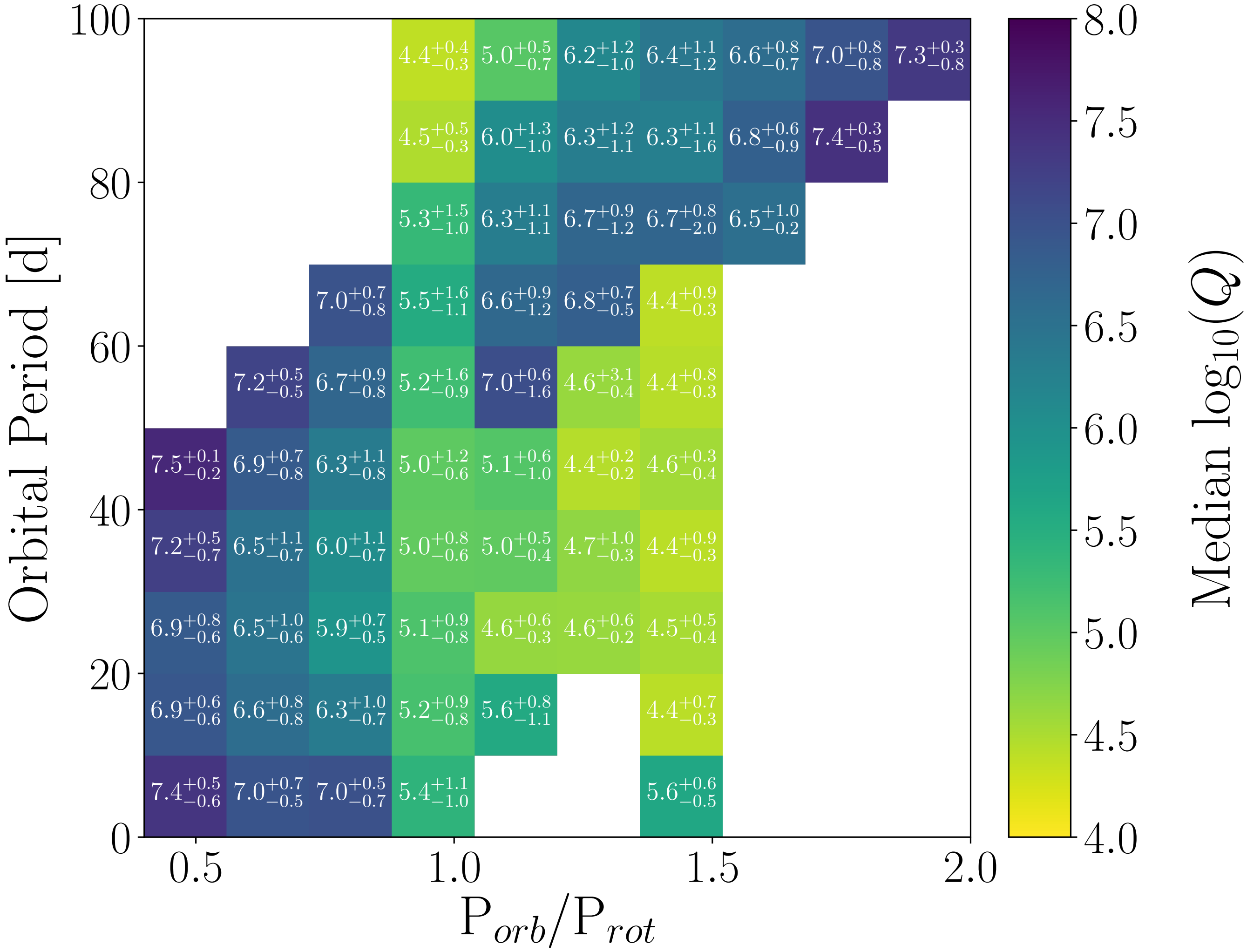

Figure 8. Median $\log_{10}(Q)$ of primary stars binned by P_{orb} and P_{orb}/P_{rot} evolved using the CPL model. In each bin, we compute the median, 16%, and 84% percentiles for $\log_{10}(Q)$ and display these values. Narrow constraints imply that certain tidal parameters are required to produce that rotation state, e.g. supersynchronous rotators near $P_{orb}/P_{rot} = 1.5$ require $Q \lesssim 10^{5.5}$.

braking according to both the Matt et al. (2015) and Reiners & Mohanty (2012) magnetic braking models.

4.4.1. *Matt et al. (2015) Magnetic Braking*

There is a clear age-dependence of P_{rot} seen in the single star population with older stars rotating more slowly, a trend that is borne out in nature and is the critical assumption of gyrochronology methods that link P_{rot} to stellar ages via the magnetic braking-driven long-term spin down of low-mass stars (e.g. Skumanich 1972; Barnes 2003, 2007; Mamajek & Hillenbrand 2008; Barnes 2010; Meibom et al. 2015). The only rapidly rotating single stars are young (ages $<$ 2 Gyr) M dwarfs ($M < 0.5$ $M_\odot$) that have just reached the main sequence and have not yet experienced substantial angular momentum loss due to magnetic braking. In stark contrast, both tidal models predict a substantial population of tidally-locked fast rotators ($P_{rot} < 20$ d). Under the CPL and CTL models, 18% and 19% of simulated stars have $P_{rot} < 20$ d, respectively, compared to only 5% in the single star models. At the long P_{rot} end, the CPL model predicts a population of slow rotators with $P_{rot} \gtrsim 70$ d, a feature not seen in either the CTL or single star models, and is produced by tidal-locking in long P_{orb} binaries with low tidal Qs, e.g. Fig. 10.

4.4.2. *Reiners & Mohanty (2012) Magnetic Braking*

Similar to the Matt et al. (2015) simulations discussed above, the single star simulations display a clear age-dependence of P_{rot}. The Reiners & Mohanty (2012) model's magnetic braking transition at $M = 0.35$ $M_\odot$ produces a sharp cutoff in the $P_{rot} - M$ distribution between late M dwarfs and more massive stars. More massive stars ($M \geq 0.35$ $M_\odot$) follow a smooth $P_{rot}-$ age

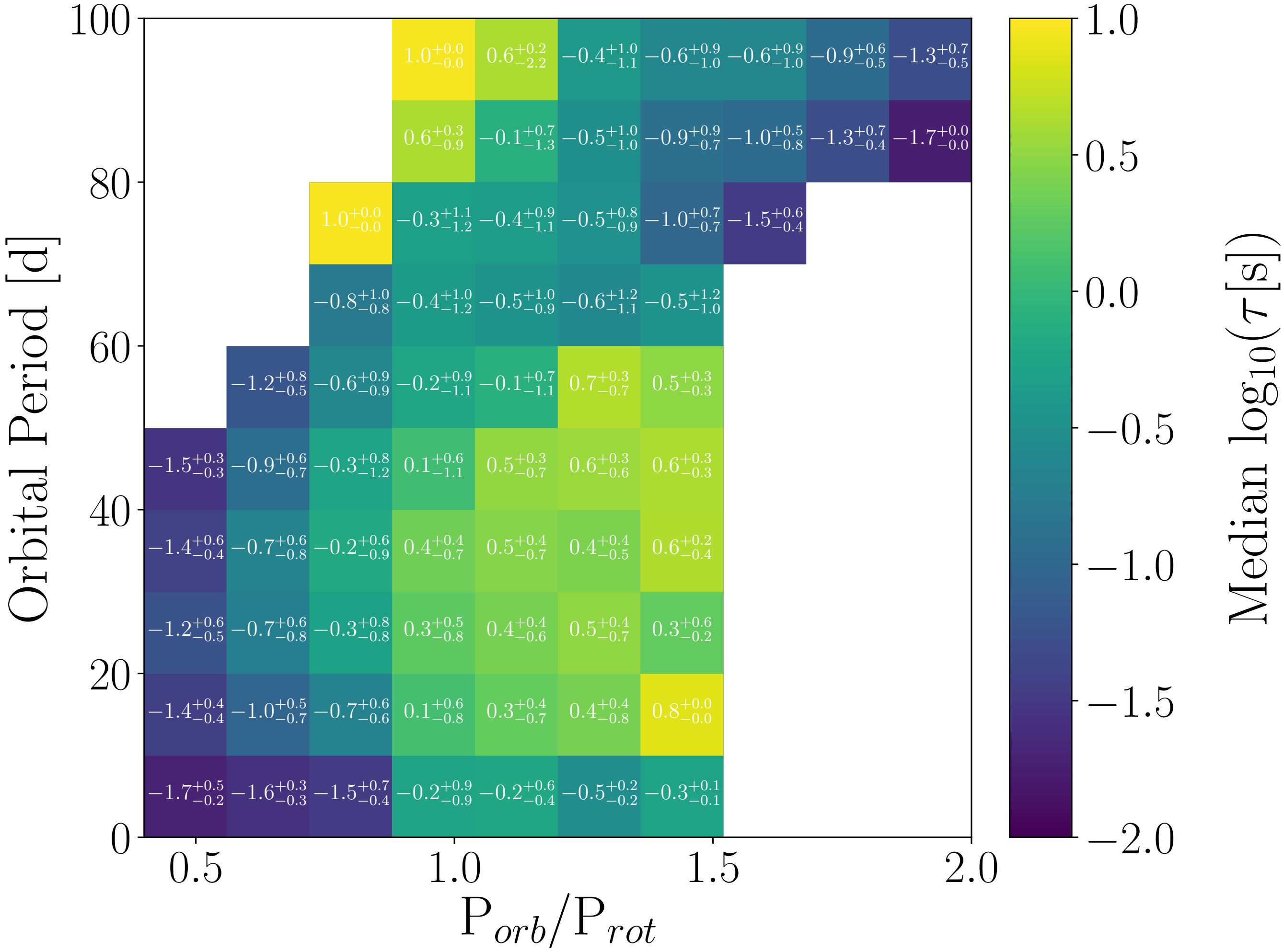

Figure 9. Same format as Fig. 8, but for $\log_{10}(\tau[s])$ under the CTL model.

sequence, while the late M dwarfs can remain rapidly rotating if they are young and in the saturated regime or extremely slowly rotating if they are older than about 4 Gyr. As in the Matt et al. (2015) model, the only rapid rotators ($P_{rot} \lesssim 20$ d) are very young stars with ages $\lesssim 2$ Gyr. The presence of extremely slowly rotating late M dwarfs, absent in the predictions of the Matt et al. (2015) model but seemingly present in nature (e.g. Newton et al. 2018), could be used as an observational discriminant between the Matt et al. (2015) and Reiners & Mohanty (2012) model, but a full investigation of which magnetic braking model accurately describes angular momentum loss in low mass stars is beyond the scope of this work.

The general trends found in the coupled stellar-tidal simulations using the Matt et al. (2015) model persist in the simulations evolved using the Reiners & Mohanty (2012) model, demonstrating that these findings are not magnetic braking model-dependant, but rather a generic result of the interaction between magnetic braking and tidal torques in low-mass binaries. Both the CPL and CTL simulations display a clear single-star magnetic braking-dominated sequence, but as before, tidally-locked binaries appear across a wide range of P_{rot} and primary star masses. Both the CPL and CTL model tidally-lock many short P_{orb} stars into rapid rotation across all masses, with both models predicting 23% of stars have $P_{rot} < 20$ d, compared to 11% of single-stars, mostly for late M dwarfs in the latter case. As shown above, the CTL model predicts that binaries can strongly tidally-interact out to long P_{orb}, seen out to $P_{rot} = 80$ d, while the CPL model can tidally-lock stars out to $P_{orb} \approx 100$ d. These strong tidal interactions seen both here and in § 4.4.1 decouple P_{rot} from age in binaries, especially for rapid rotators.

4.4.3. *Impact of Binarity on Gyrochronology*

Our models predict that age does not strongly correlate with P_{rot} in low-mass binaries, especially for

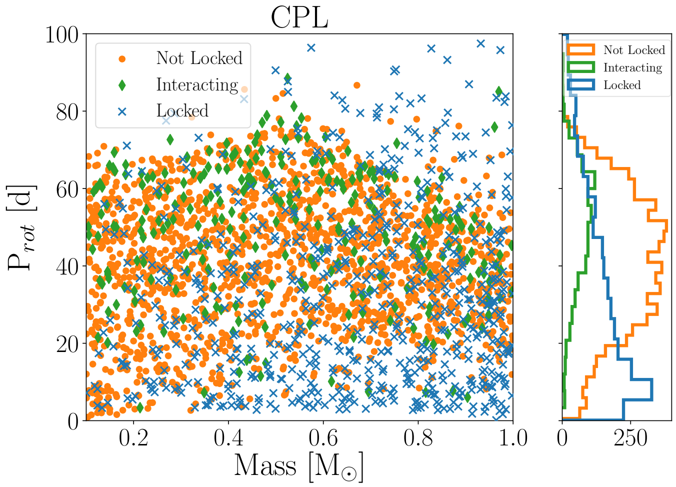

Figure 10. Rotation state for tidally-locked (blue, $P_{rot} = P_{eq}$), interacting (green, P_{rot} within 10% of P_{eq} and not locked), and not locked (orange, remainder of binaries) stellar binaries. Left: P_{rot} as a function of stellar mass and age according to our CPL simulations integrated to system ages uniformly sampled over $1-7$ Gyr. Right: Marginalized P_{rot} distribution for each case.

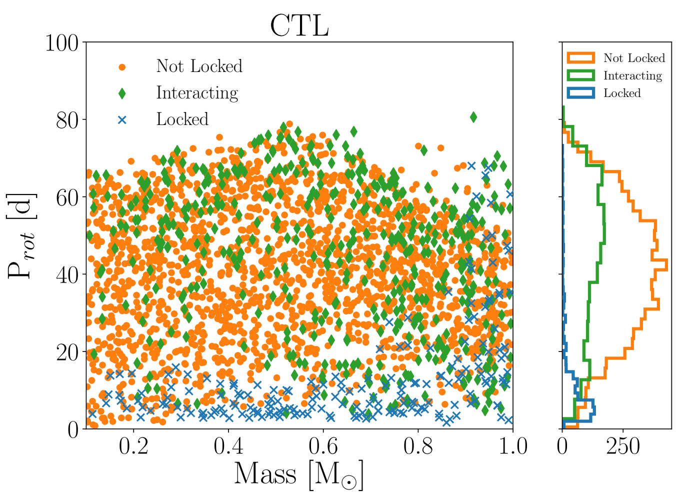

Figure 11. Same format as Fig. 10, but for the CTL simulations.

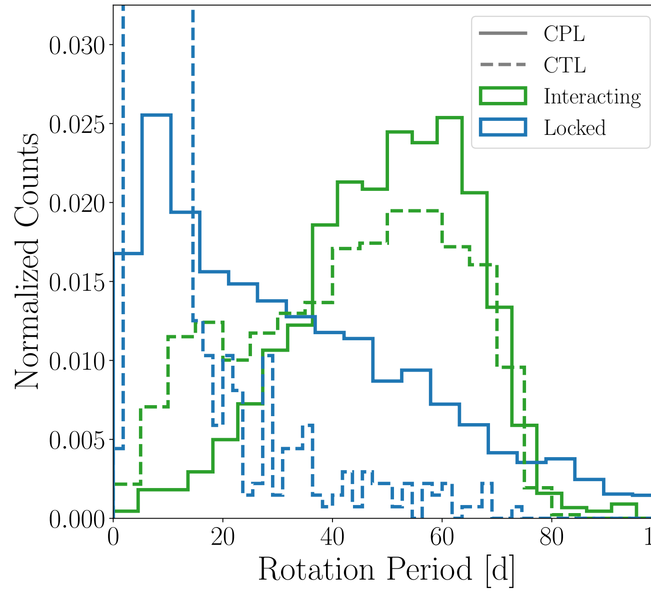

Figure 12. P_{rot} distribution for tidally-locked (blue) and interacting (green, P_{rot} within 10% of P_{eq} and not locked) binaries according to the CPL (solid line) and CTL (dashed line) models.

$P_{orb} < 20$ d. Under the Matt et al. (2015) model discussed in § 4.4.1, the median ages and 68% interval for fast rotators ($P_{rot} \lesssim$20 d) are $2.8^{+2.9}_{-1.5}$ Gyr and $3.1^{+2.6}_{-1.8}$ Gyr according to the CPL and CTL models, respectfully, compared to much younger single stars with ages of $1.3^{+0.5}_{-0.3}$ Gyr. Similarly for the models evolved with the Reiners & Mohanty (2012) model discussed in § 4.4.2, the median ages and 68% interval for fast rotators are $2.6^{+2.8}_{-1.3}$ Gyr and $2.7^{+2.7}_{-1.4}$ Gyr according to the CPL and CTL models, respectfully, compared to single stars with ages of $1.7^{+0.9}_{-0.5}$ Gyr, We highlight this stark dichotomy between the age distribution of single and double stars in Fig. 15 by plotting a histogram of system ages from Fig. 13 for single or primary stars in binaries with $P_{rot} < 20$ d.

Tidal torques pose a fundamental problem for inferring ages of stars via gyrochronlogy. Regardless of the choice of equilibrium tidal model or magnetic braking model, stellar binaries readily tidally-lock, or at least strongly tidally-interact, across a wide range of P_{orb} and primary star masses, decoupling P_{rot} from age. For example, if one observed a rapidly rotating star with $P_{rot} \lesssim$20 d, gyrochronology models would predict ages $\lesssim$2 Gyr. If a rapidly-rotating star is actually an unresolved binary, it would likely be tidally-locked, decoupling P_{rot} from age, causing the predictions of gyrochronology models to fail as its age could be at least several Gyrs, e.g. Fig. 15. This effect is most likely to manifest in rapid rotators ($P_{rot} < 20$ d), but persists across all P_{rot} up to 100 d, producing a significant contaminating signal, e.g. Fig. 13 and Fig. 14.

In general, it is difficult to accurately determine if a source is single star or a stellar binary via longterm photometric monitoring as only a small fraction of stars in binaries will occult one another. Observations of the binarity of field stars by Raghavan et al. (2010) and Duchêne & Kraus (2013) indicate that roughly half of stars are in stellar binaries, with 10% of these binaries having $P_{orb} \lesssim$100 d, suggesting that unless one accounts for binarity, stellar binaries will produce a non-negligible

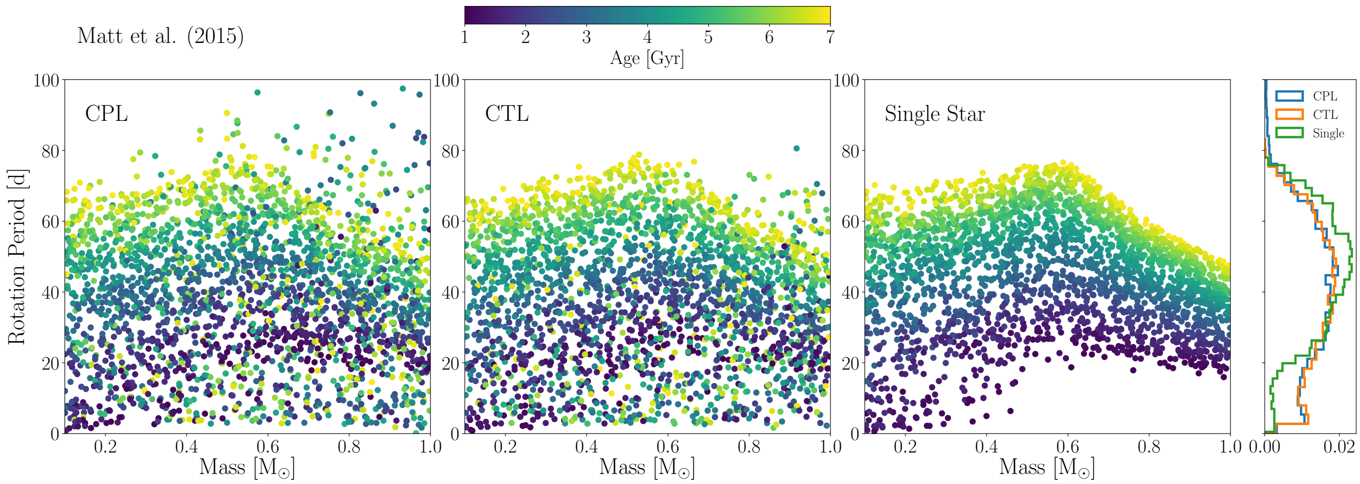

Figure 13. P$_{rot}$ as a function of stellar mass and age according to our CPL (left), CTL (left center), and single star (right center) simulations integrated to system ages uniformly sampled over $1 - 7$ Gyr using the Matt et al. (2015) magnetic braking model. For each case, we only plot 2,500 systems for clarity but account for all systems when computing the marginalized distributions. Right: The P$_{rot}$ distribution for each case, marginalized over stellar mass.

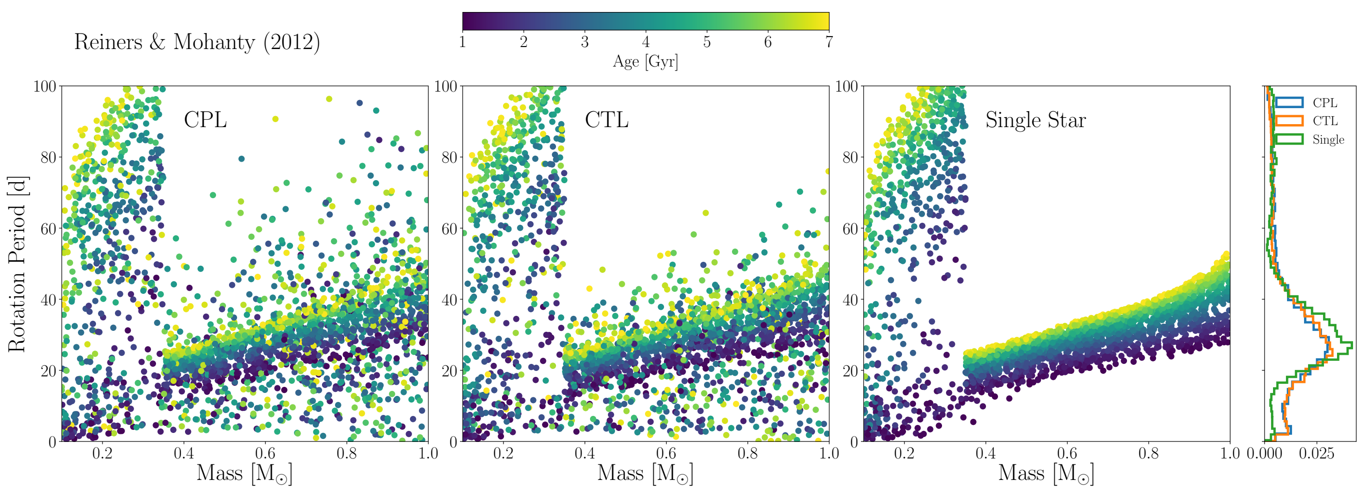

Figure 14. Same format as Fig. 13, but evolved using the Reiners & Mohanty (2012) magnetic braking model.

contaminating signal in any study of stellar rotation periods and any ages inferred via gyrochronlogy are potentially subject to systematic errors. Moreover, this problem could be more significant as Simonian et al. (2018) found that most rapid rotators with P$_{rot}$ ≤ 7.5 d in the *Kepler* field are likely photometric binaries, suggesting that binary contamination in P$_{rot}$ studies could be widespread. We caution that any application of gyrochronlogy methods to predict ages for stars, especially those with P$_{rot}$ $\lesssim$20 d, should rule out or account for stellar binarity, or otherwise risk deriving systematically incorrect ages.

Furthermore, any study of the angular momentum evolution of a stellar population will be flawed unless one robustly accounts for binarity. Tidal torques do not just produce spin-orbit synchronization at short P$_{orb}$, but can produce a rich variety of rotation states that deviate from the expected long-term spin-down experienced by single stars, e.g. Fig. 8 and Fig. 9. We recommend that the application, or calibration, magnetic braking models to a sample of stellar rotation periods control for binarity.

4.5. *Comparison to Kepler*

We compare our simulation results using both tidal models and the Matt et al. (2015) magnetic braking model to P$_{rot}$ measurements of primary stars in *Kepler* low-mass eclipsing stellar binaries by Lurie et al. (2017). The purpose of this comparison is to see if our model predictions, which by design populate a wide, but physically-plausible, region of parameter space, can

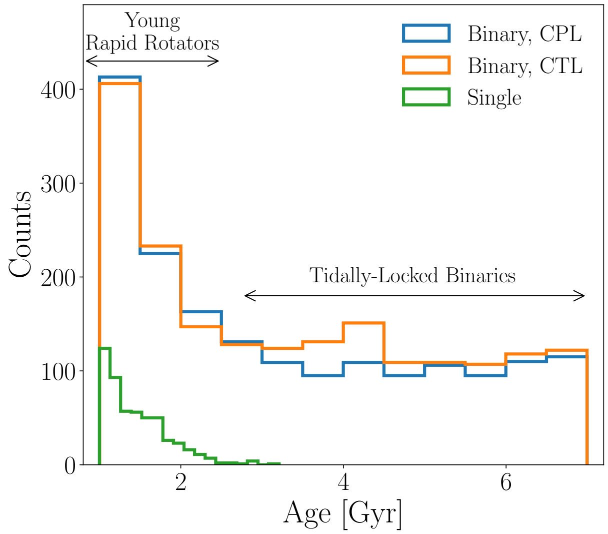

Figure 15. Histogram of rapidly-rotating ($P_{rot} < 20$ d) stellar ages for single and primary stars in binaries from Fig. 13. Rapidly-rotating single stars must be young (ages $\lesssim$2 Gyr), while tidally-locked rapidly-rotating binaries exhibit a wide range of ages.

reproduce features observed in the data. Lurie et al. (2017) measured 816 rotation periods for primary stars in *Kepler* EBs with star spot modulations and visually inspected each light curve to ensure their accuracy. The Lurie et al. (2017) dataset is the largest homogenous set of P_{rot} measurements available for low-mass stellar binaries and represents the state of the art benchmark for studies of the influence of tides on P_{rot} in stellar binaries. We compare our results to the $P_{1,min}$ P_{rot} values reported by Lurie et al. (2017) as the authors demonstrated that these values are likely to be close to the equatorial P_{rot} that we track in our simulations. In Fig. 16, we display P_{orb}/P_{rot} as a function of P_{orb} for both the CPL and CTL models where each simulation was integrated to an age uniformly sampled over $1 - 7$ Gyr, consistent with ages of *Kepler* field stars (Chaplin et al. 2014), and the Lurie et al. (2017) data.

Both tidal models qualitatively reproduce most features seen in the Lurie et al. (2017) data, especially at short P_{orb}. Nearly all simulated binaries with $P_{orb} < 4$ d have circularized orbits and synchronized spins due to strong tidal torques at short stellar separations, in agreement with the Lurie et al. (2017) observations. At very short P_{orb}, in the absence of a perturbing tertiary companion, circularization and synchronization is the inevitable end state for low-mass binaries, in good agreement with theoretical predictions (Counselman 1973). For $P_{orb} \gtrsim$4 d, our models produce large populations of subsynchronous rotators. Although Lurie et al. (2017) argues that differential rotation creates the subsynchronous population, we find that the competition between weak tidal torques and magnetic braking described in § 4.1 naturally produces subsynchronous rotators. For example under the CTL model, our simulated subsynchronous binaries have systematically weaker tidal torques than the rest of the sample, as expected, as they have a median $\tau = 0.17$ s, compared to the median $\tau = 0.47$ s for the tidally-locked supersynchronous population.

The CPL model can produce subsynchronous rotators similar to the observed population with $10 \lesssim P_{orb} \lesssim 20$ d, but struggles to populate the prominent cluster of subsynchronous rotators at $P_{orb}/P_{rot} \approx 0.9$ for $P_{orb} < 10$ d observed by Lurie et al. (2017). The CTL model, on the other hand, populates a much wider swath of parameter space than the CPL model can, qualitatively reproducing many clusters seen in the Lurie et al. (2017) data. Lurie et al. (2017) find that 15% of their subsynchronous population with $2 < P_{orb} < 10$ days has $P_{orb}/P_{rot} \in [0.84, 0.92]$, the cluster of stars those authors identified near $P_{orb}/P_{rot} = 0.9$, compared with 9% of our CTL population, suggesting that subsynchronous rotation is a common outcome of stellar-tidal evolution in low-mass binaries. Furthermore in the same P_{orb} regime, Lurie et al. (2017) find that 72% of their population has $P_{orb}/P_{rot} \in [0.92, 1.2]$, compared with 72% of our CTL population, in good agreement. In comparison, the CPL model predicts 68% of the population has $P_{orb}/P_{rot} \in [0.92, 1.2]$ and 2% has $P_{orb}/P_{rot} \in [0.84, 0.92]$ for $2 < P_{orb} < 10$ d, producing a population of synchronized binaries similar to what is seen in the *Kepler* EB population, but not the subsynchronous cluster identified by Lurie et al. (2017).

The CPL model cannot produce the cluster of supersynchronous rotators with $P_{orb}/P_{rot} \lesssim$1.1 for $P_{orb} < 10$ d present in the Lurie et al. (2017) data. Instead, owing to the its discrete P_{eq}, the CPL model predicts that all tidally-locked supersynchronous rotators lie on the line $P_{orb}/P_{rot} = 1.5$. This prediction is inconsistent with the data as no obvious spin-orbit commensurablity, aside from 1:1 synchronization, is present in the Lurie et al. (2017) data, likely because stellar convective envelopes lack a fixed shape, making resonant coupling difficult unless coupling occurs with internal gravity or pressure modes (Burkart et al. 2014; Lurie et al. 2017). On the other hand, the CTL model produces a large number of supersynchronous binaries with eccentric orbits. These systems have tidally-locked but their orbits have not yet circularized, even though they likely experience strong tidal torques at short separations, because the tidal locking time scale is 2-3 orders of magnitude less than the circularization timescale (Mazeh 2008).

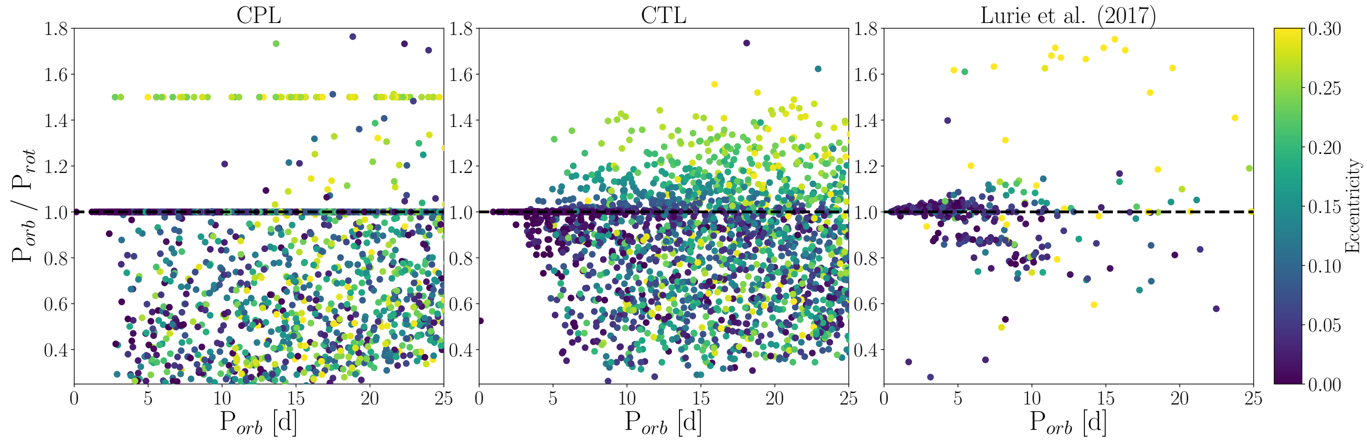

Figure 16. P_{orb}/P_{rot} as a function of P_{orb} according to the CPL model (left) and the CTL model (middle), and Lurie et al. (2017) *Kepler* EB observations (right). All points are colored by e. In the right panel, the *Kepler* EBs at low P_{orb} and low P_{orb}/P_{rot} are likely either brown dwarfs or exoplanets (Lurie et al. 2017), and hence are not modeled by our simulations, so we do not consider them, but we display them for completeness.

Both models predict a large number of extremely subsynchronous rotators with $P_{orb}/P_{rot} < 0.7$ across all P_{orb} that is not seen in the Lurie et al. (2017) data. Magnetic braking and age combine to produce the lower limit of this subsynchronous population. The limit is a line of nearly constant $P_{rot} \approx 60$ d set by how much a star can spin down via magnetic braking in the weak tides regime over 7 Gyr, the longest age considered in our simulations. Our choice of prior distributions for both Q and τ permit very weak tidal interactions, e.g. $Q \gtrsim 10^7$ and $\tau < 0.1$ s, that likely gives rise to this extremely subsynchronous population and suggests that our prior does not reflect the underlying distribution of stellar tidal parameters in nature. Alternatively, the data could be incomplete where our models predict slowly-rotating subsynchronous rotators as the photometric amplitude of star spot modulations tends to decrease with increasing P_{rot}, making reliable rotation periods difficult to detect (McQuillan et al. 2014; Lurie et al. 2017; Reinhold et al. 2018).

Both tidal models reproduce many features observed in the *Kepler* EB distribution, suggesting that our model is a fair representation of the dynamical interactions of tidally-evolving, low-mass stellar binaries. Our comparison between theory and observations is limited, however. The Lurie et al. (2017) P_{rot} data lack uncertainties and Lurie et al. (2017) used transit durations and ingress/egress times to approximate the EB orbital e, leading to inaccurate e determinations. Furthermore, biases in the data, e.g. the lack of long P_{orb} binaries, inhibit our ability to robustly compare our predictions with the data. We discuss this point further in § 4.7 and offer observational tests to discriminate between which of the two models better describes tidal interactions in low-mass binaries in § 4.6.

4.6. *CPL or CTL?*

Accurate measurements of P_{rot} and e, especially out to long P_{orb}, can potentially discriminate between which equilibrium tidal model best describes tidal interactions in low-mass stellar binaries. Here, we outline three observational tests that can discriminate between the two models. The first two require obtaining a series of time-resolved spectra over full orbital phase of short P_{orb} supersynchronous binaries, i.e. those identified by Lurie et al. (2017), to compute radial velocities over the binary's orbit. Combined with *Kepler* photometry, one can derive much more robust e constraints than those computed using the transit approximations in Lurie et al. (2017).

The first test considers binaries with $P_{orb} < 10$ d that are likely tidally-locked on eccentric orbits, but with $e < 0.23$. In this e regime, the CPL model predicts that the majority of systems are tidally-locked into synchronous rotation and does not permit a supersynchronous rotation state, e.g. Eqn. (21). The CTL model, however, predicts a continuum of supersynchronous rotators on eccentric orbits, e.g. Eqn. (23). Supersynchronous rotation that is not due to tidal interactions can occur in extremely young, rapidly rotating systems that are still contracting along the pre-main sequence, or that have recently reached the main sequence. These young, supersynchronous rotators are unlikely to be tidally-locked, usually have $P_{orb}/P_{rot} > 1.5$, and do not stay supersynchronous for long given that solar mass pre-main sequence lifetimes are $\lesssim$100 Myr, distinguishing them from tidally-locked binaries (see Fig. 16). If supersynchronous rotation is observed in binaries with

$P_{orb} < 10$ d, $P_{orb}/P_{rot} < 1.5$, and $0 < e \lesssim 0.23$, it is evidence in favor of the CTL model over our discrete CPL model.

Second, for tidally-locked binaries with $e > 0.23$, the CPL model predicts supersynchronous rotation in the form of a 3:2 spin-orbit comensurability, e.g. the line at $P_{orb}/P_{rot} = 1.5$ seen in the left panel of Fig. 16, and no other spin state is permitted, compared to the continuum of supersynchronous rotation states in eccentric tidally-locked rotators predicted by the CTL model. If a substantial clustering of stellar binaries with $P_{orb}/P_{rot} = 1.5$ is observed, it would be strong evidence in favor of the CPL model. It is unclear, however, if low-mass binary stars can even lock into spin-orbit resonances, such as those discussed in Rodríguez et al. (2012), as stellar convective envelopes lack a fixed shape (Burkart et al. 2014; Lurie et al. 2017). There is no obvious clustering of stars near any spin-orbit resonance, aside from 1:1 spin-orbit synchronization in the Lurie et al. (2017) *Kepler* EB data. The lack of uncertainties on the Lurie et al. (2017) P_{rot} measurements and their poor eccentricity constrains, however, prohibit us from making any distinction between models conclusive. More robust phase-resolved spectroscopic e constrains would aid in this discriminaton between models, as would determinations of P_{rot} with uncertainties, perhaps using a Gaussian process model as was done by Angus et al. (2018).

These two tests can fail to discriminate between the CPL and CTL model, however, if the CPL model P_{eq} is a continuous function of e, e.g. Eqn. (22), as was argued by Goldreich (1966) and derived by Murray & Dermott (1999). In such a case, one would need a large number of accurate and precise measurements P_{orb} and e, with robust uncertainties, for tidally-interacting binaries to discriminate between the CPL and CTL continuous P_{eq}, e.g. Eqn. (22) versus Eqn. (23). In practice, this is extremely observationally expensive as it requires extensive photometric and spectroscopic observations of many binaries. Since there is no obvious clustering of *Kepler* EBs near any spin-orbit resonance, the above two tests are likely insufficient. We offer a third observational test that provides the best method to discriminate between models.

As shown in § 4.3, the detection of tidally-locked binaries with $P_{rot} \gtrsim 80$ d would provide strong evidence in favor of the CPL model, as the CTL model is unlikely to tidally-lock binaries past $P_{orb} \approx 20$ d and cannot tidally-lock stars beyond $P_{orb} \approx 80$ d, even with extreme τ, e.g. Fig. 11. The CPL model, however, readily tidally-locks binaries out to $P_{orb} \approx 100$ d. We recommend observers try to measure P_{rot} and e in binaries out to $P_{orb} = 100$ d to test this hypothesis, but we note that detecting P_{rot} for such slow rotators can be difficult due to small star spot modulation amplitudes (McQuillan et al. 2014; Lurie et al. 2017; Reinhold et al. 2018). Long term spectroscopic monitoring may be warranted in such cases.

4.7. *Inferring Stellar and Binary Properties from Kepler*

In principle, we could have conditioned our model on the Lurie et al. (2017) data to infer population-level properties of stellar binaries, such as tidal Q and τ values for stars, perhaps as a function of stellar mass, or the initial binary P_{orb} distribution, using hierarchical probabilistic modeling instead of qualitatively comparing of our simulations with the data. Such an analysis is beyond the scope of this work, however. Furthermore, the biases in the Lurie et al. (2017) data are not well known. For example, the bias of the obvious lack of longer P_{orb} binaries in the Lurie et al. (2017) data arises from the fact that it is difficult to detect binaries with longer P_{orb} in a finite time window via the transit method as longer P_{orb} systems transit fewer times. What is not known, however, is how this bias impacts the completeness of binary detections as a function of P_{orb}, nor is the completeness known as a function of stellar P_{rot}. Unconstrained observational biases, combined with the lack of P_{rot} uncertainties, potentially inaccurate binary eccentricities, and lack of binary masses and ages makes it difficult to directly compare our simulations with the data to robustly infer properties of low-mass binaries.

Instead, one could use our model to infer tidal properties for individual systems with well-constrained properties. For example, Kepler-47 (Orosz et al. 2012) is a low-mass binary whose primary star rotates subsynchronously. This system has been extensively monitored via photometry and spectroscopy because it harbors multiple transiting circumbinary planets, and as a result has well-constrained properties. One could infer the tidal properties of this binary, perhaps in a Markov Chain Monte Carlo framework, by directly comparing simulation results with the observed stellar and orbital properties, given the observational uncertainties and reasonable prior probability distributions for parameters like the initial binary e. This analysis, however, is also beyond the scope of this work and we leave it for future endeavors.

5. DISCUSSION

In this work, we probed the long-term angular momentum evolution of low-mass stellar binaries, with a focus on P_{rot} in short and intermediate P_{orb} binaries.

We considered the impact of two common equilibrium tidal models, two magnetic braking models, and stellar evolution. We performed a large suite of simulations for binaries with physically-motivated initial conditions out to P_{orb} = 100 and across a wide range of tidal dissipation parameters to examine the competition between tidal torques and magnetic braking for controlling the stellar P_{rot} evolution.

In our simulations, nearly all binaries with $P_{orb} \lesssim 4$ d have tidally-synchronized spins and circularized orbits, in good agreement with observations of *Kepler* EBs and binaries in the field. We showed for $P_{orb} \gtrsim 4$ d, primary stars in stellar binaries can rotate subsynchronously for Gyrs due to the competition between tidal torques and magnetic braking, or supersynchronously if they tidally-lock on eccentric orbits. Our predictions are not strongly dependant on the choice of magnetic braking model, but rather are generic outcomes of the interaction between magnetic braking and tidal torques. Both the CPL and CTL equilibrium tidal models predict that binaries tidally-interact at longer P_{orb} than have previously been considered, out to $P_{orb} \approx 80$ d. Many binaries with $P_{orb} \lesssim 20$ d tidally-lock according to both models, in good agreement with previous results, but the CPL model predicts that binaries can readily tidally-lock out to $P_{orb} \approx 100$ d. Tidal interactions can cause P_{rot} evolution in stellar binaries to differ from the long-term spin down due to magnetic braking experienced by single stars, decoupling P_{rot} from age. In tidally-interacting binaries, gyrochronology, the technique of linking stellar P_{rot} to age, likely fails. We caution that any application of gyrochronlogy methods to stars, especially those with $P_{rot} \lesssim 20$ d, should account for the possibility of stellar binarity to prevent deriving incorrect ages.

We compare the predictions of both the CPL and CTL models with observations of P_{rot} and P_{orb} of *Kepler* EBs by Lurie et al. (2017) and find that both can qualitatively reproduce many features seen in the data, validating our approach and suggesting that equilibrium tidal models can accurately model stellar-tidal evolution in low-mass stellar binaries. The lack of uncertainties on P_{rot}, the approximate orbital eccentricities derived by Lurie et al. (2017), and unconstrained completeness estimates prevent us from discriminating between which tidal model best describes tidal torques in low-mass binaries and from inferring tidal properties of low-mass stars given the *Kepler* EB data. We described three observational tests that can distinguish between which equilibrium tidal model better describes tidal interactions in low-mass stellar binaries. To perform these tests, we recommend that observers make additional measurements of e and P_{rot} in binaries, especially at long P_{orb} out to 100 d, although we note that these are non-trivial observations.

Our theoretical predictions outline a critical point: one cannot simply observe a short P_{orb} binary on a circular orbit and assume synchronization, nor can one observe a binary with $P_{orb} \gtrsim 20$ d and assume that tides have not impacted that system's angular momentum evolution. Stellar-tidal interactions can produce synchronous and subsynchronous rotation for short P_{orb} binaries on circular orbits, e.g. Fig. 4, depending on the age of the system, e.g. Fig. 6, and the strength of tidal dissipation, e.g. Fig. 8 and Fig. 9. Understanding the long-term angular momentum evolution of stellar binaries out to $P_{orb} = 100$ d requires detailed modeling of its coupled-stellar tidal evolution, and characterizing tidal dissipation parameters, e.g. how Q and τ vary from star-to-star. Many new eclipsing stellar binaries will be discovered by TESS (e.g. Sullivan et al. 2015; Matson et al. 2018) and in analysis of K2 data. Obtaining precise orbital and rotational constraints for stellar binaries will permit detailed characterization of tidal interactions between low-mass stars and shed light into the long-term angular momentum evolution in stellar binaries.

This work was facilitated though the use of advanced computational, storage, and networking infrastructure provided by the Hyak supercomputer system and funded by the Student Technology Fund at the University of Washington. DPF was supported by NASA Headquarters under the NASA Earth and Space Science Fellowship Program - Grant 80NSSC17K0482. RB acknowledges support from the NASA Astrobiology Institute's Virtual Planetary Laboratory under Cooperative Agreement number NNA13AA93A. JRAD acknowledges support from the DIRAC Institute in the Department of Astronomy at the University of Washington. The DIRAC Institute is supported through generous gifts from the Charles and Lisa Simonyi Fund for Arts and Sciences, and the Washington Research Foundation.

APPENDIX

A. ANALYTIC TORQUE BALANCE

Here we derive the equation for the stellar P_{rot} at which tidal torques balance magnetic braking discussed in § 4.1.1. As in § 4.1.1, we assume that both stars have $M = 1 M_{\odot}$, 0 obliquity, and we assume a circular binary orbit. We assume that the torque balance occurs while the stars are on the main sequence, where stellar properties change slowly, so the angular momentum evolution is controlled by the balance between tidal torques and magnetic braking, not stellar radius contraction. Under this assumption, we can set $R = 1R_\odot$ and assume constant moments of inertia. For simplicity, we assume that magnetic braking proceeds under the Matt et al. (2015) model and the CTL model describes tidal torques.

As discussed in § 4.1.1, both stars are in the unsaturated rotation regime, so the torque due to magnetic braking is given by Eqn. (2), which under the aforementioned assumptions, reduces to

$$\left.\frac{dJ}{dt}\right|_{MB} = -C_{MB}\left(\frac{P_{rot,\odot}}{P_{rot}}\right)^3 \tag{A1}$$

where $\mathrm{P}_{rot} = 2\pi/\omega$ and $C_{MB} = 9.5 \times 10^{30}$ ergs (Matt et al. 2015).

Under the CTL model and our assumptions, the change in rotation rate due to tidal torques, Eqn. 17, reduces to

$$\left.\frac{d\omega}{dt}\right|_{tides} = \frac{\mathrm{P}_{orb}\mathrm{Z}_{CTL}}{2\pi M r_g^2 R^2}\left(1 - \frac{\mathrm{P}_{orb}}{\mathrm{P}_{rot}}\right) \tag{A2}$$

where $\mathrm{P}_{orb} = 2\pi/n$. For fixed moment of inertia, $dJ/dt = I d\omega/dt$, and after inserting Eqn. 19 for Z_{CTL}, the tidal torque on the stellar rotations becomes

$$\left.\frac{dJ}{dt}\right|_{tides} = \frac{C_{tides}k_2\tau}{\mathrm{P}_{orb}^5}\left(1 - \frac{\mathrm{P}_{orb}}{\mathrm{P}_{rot}}\right). \tag{A3}$$

where $C_{tides} = 24\pi^5 R_\odot^5/G$.

The torques due to tides and magnetic braking balance when $\frac{dJ}{dt}|_{tides} + \frac{dJ}{dt}|_{MB} = 0$,

$$\frac{C_{tides}k_2\tau}{\mathrm{P}_{orb}^5}\left(1 - \frac{\mathrm{P}_{orb}}{\mathrm{P}_{rot}}\right) - C_{MB}\left(\frac{P_{rot,\odot}}{P_{rot}}\right)^3 = 0. \tag{A4}$$

By specifying P_{orb} and the product, $k_2\tau$, we can numerically solve Eqn. (A4) for the P_{rot} at which torques due to magnetic braking and tides balance, often producing subsynchronous rotation as seen in Fig. 3 and our simulations in § 4.1.

REFERENCES

Abt, H. A., & Boonyarak, C. 2004, ApJ, 616, 562

Agüeros, M. A., Covey, K. R., Lemonias, J. J., et al. 2011, ApJ, 740, 110

Angus, R., Morton, T., Aigrain, S., Foreman-Mackey, D., & Rajpaul, V. 2018, MNRAS, 474, 2094

Baraffe, I., Homeier, D., Allard, F., & Chabrier, G. 2015, A&A, 577, A42

Barker, A. J., & Ogilvie, G. I. 2009, MNRAS, 395, 2268

Barnes, R. 2017, ArXiv e-prints, arXiv:1708.02981

Barnes, R., Mullins, K., Goldblatt, C., et al. 2013, Astrobiology, 13, 225

Barnes, R., Deitrick, R., Luger, R., et al. 2016, ArXiv e-prints, arXiv:1608.06919

Barnes, R., Luger, R., Deitrick, R., et al. 2018, in AAS/Division for Planetary Sciences Meeting Abstracts, Vol. 50, AAS/Division for Planetary Sciences Meeting Abstracts, 413.03

Barnes, S. A. 2003, ApJ, 586, 464

—. 2007, ApJ, 669, 1167

—. 2010, ApJ, 722, 222

Bate, M. R. 2000, MNRAS, 314, 33

Bate, M. R., Bonnell, I. A., & Bromm, V. 2002, MNRAS, 336, 705

Bolmont, E., & Mathis, S. 2016, Celestial Mechanics and Dynamical Astronomy, 126, 275

Bonnell, I. A., & Bate, M. R. 1994, MNRAS, 271, astro-ph/9411081

Burkart, J., Quataert, E., & Arras, P. 2014, MNRAS, 443, 2957

Chaplin, W. J., Basu, S., Huber, D., et al. 2014, ApJS, 210, 1

Claret, A., Gimenez, A., & Cunha, N. C. S. 1995, A&A, 299, 724

Counselman, III, C. C. 1973, ApJ, 180, 307
Cranmer, S. R., & Saar, S. H. 2011, ApJ, 741, 54
Darwin, G. H. 1880, Philosophical Transactions of the Royal Society of London Series I, 171, 713
Douglas, S. T., Agüeros, M. A., Covey, K. R., & Kraus, A. 2017, ApJ, 842, 83
Duchêne, G., & Kraus, A. 2013, ARA&A, 51, 269
Dunn, O. J. 1961, Journal of the American Statistical Association, 56, 52. https://www.tandfonline.com/doi/abs/10.1080/01621459.1961.10482090
Ferraz-Mello, S., Rodríguez, A., & Hussmann, H. 2008, Celestial Mechanics and Dynamical Astronomy, 101, 171
Fleming, D. P., Barnes, R., Graham, D. E., Luger, R., & Quinn, T. R. 2018, ApJ, 858, 86
Fleming, D. P., & Quinn, T. R. 2017, MNRAS, 464, 3343
Gaia Collaboration, Prusti, T., de Bruijne, J. H. J., et al. 2016, A&A, 595, A1
Goldreich, P. 1966, AJ, 71, 1
Goldreich, P., & Peale, S. 1966, AJ, 71, 425
Goldreich, P., & Soter, S. 1966, Icarus, 5, 375
Greenberg, R. 2009, ApJL, 698, L42
Habets, G. M. H. J., & Zwaan, C. 1989, A&A, 211, 56
Haisch, Jr., K. E., Lada, E. A., & Lada, C. J. 2001, ApJL, 553, L153
Hamers, A. S., Perets, H. B., & Portegies Zwart, S. F. 2016, MNRAS, 455, 3180
Heller, R., Leconte, J., & Barnes, R. 2011, A&A, 528, A27
Herbst, W., Bailer-Jones, C. A. L., & Mundt, R. 2001, ApJL, 554, L197
Herbst, W., Bailer-Jones, C. A. L., Mundt, R., Meisenheimer, K., & Wackermann, R. 2002, A&A, 396, 513
Howell, S. B., Sobeck, C., Haas, M., et al. 2014, PASP, 126, 398
Hurley, J. R., Tout, C. A., & Pols, O. R. 2002, MNRAS, 329, 897
Hut, P. 1981, A&A, 99, 126
Ivanova, N., Belczynski, K., Fregeau, J. M., & Rasio, F. A. 2005, MNRAS, 358, 572
Jackson, B., Barnes, R., & Greenberg, R. 2009, ApJ, 698, 1357
Jackson, B., Greenberg, R., & Barnes, R. 2008, ApJ, 678, 1396
Keppens, R. 1997, A&A, 318, 275
Khaliullin, K. F., & Khaliullina, A. I. 2011, MNRAS, 411, 2804
Leconte, J., Chabrier, G., Baraffe, I., & Levrard, B. 2010, A&A, 516, A64
Levato, H. 1974, A&A, 35, 259
Lurie, J. C., Vyhmeister, K., Hawley, S. L., et al. 2017, AJ, 154, 250
Mamajek, E. E., & Hillenbrand, L. A. 2008, ApJ, 687, 1264
Mardling, R. A., & Aarseth, S. J. 2001, MNRAS, 321, 398
Martin, D. V., Mazeh, T., & Fabrycky, D. C. 2015, MNRAS, 453, 3554
Matson, R. A., Howell, S. B., & Ciardi, D. 2018, arXiv e-prints, arXiv:1811.02108
Matt, S. P., Brun, A. S., Baraffe, I., Bouvier, J., & Chabrier, G. 2015, ApJL, 799, L23
Mazeh, T. 2008, in EAS Publications Series, Vol. 29, EAS Publications Series, ed. M.-J. Goupil & J.-P. Zahn, 1–65
McQuillan, A., Mazeh, T., & Aigrain, S. 2014, ApJS, 211, 24
Meibom, S., Barnes, S. A., Platais, I., et al. 2015, Nature, 517, 589
Meibom, S., & Mathieu, R. D. 2005, ApJ, 620, 970
Meibom, S., Mathieu, R. D., & Stassun, K. G. 2006, ApJ, 653, 621
Mestel, L. 1968, MNRAS, 138, 359
Moe, M., & Kratter, K. M. 2018, ApJ, 854, 44
Muñoz, D. J., & Lai, D. 2015, Proceedings of the National Academy of Science, 112, 9264
Murray, C. D., & Dermott, S. F. 1999, Solar system dynamics
Newton, E. R., Mondrik, N., Irwin, J., Winters, J. G., & Charbonneau, D. 2018, AJ, 156, 217
Ogilvie, G. I., & Lin, D. N. C. 2007, ApJ, 661, 1180
Orosz, J. A., Welsh, W. F., Carter, J. A., et al. 2012, Science, 337, 1511
Raghavan, D., McAlister, H. A., Henry, T. J., et al. 2010, ApJS, 190, 1
Reiners, A., & Mohanty, S. 2012, ApJ, 746, 43
Reinhold, T., Bell, K. J., Kuszlewicz, J., Hekker, S., & Shapiro, A. I. 2018, arXiv e-prints, arXiv:1810.11250
Reinhold, T., Reiners, A., & Basri, G. 2013, A&A, 560, A4
Repetto, S., & Nelemans, G. 2014, MNRAS, 444, 542
Ricker, G. R., Winn, J. N., Vanderspek, R., et al. 2014, in Proc. SPIE, Vol. 9143, Space Telescopes and Instrumentation 2014: Optical, Infrared, and Millimeter Wave, 914320
Rodríguez, A., Callegari, N., Michtchenko, T. A., & Hussmann, H. 2012, MNRAS, 427, 2239
Rodríguez-Ledesma, M. V., Mundt, R., & Eislöffel, J. 2009, A&A, 502, 883
Simonian, G. V. A., Pinsonneault, M. H., & Terndrup, D. M. 2018, ArXiv e-prints, arXiv:1809.02141
Skumanich, A. 1972, ApJ, 171, 565
Stassun, K. G., Mathieu, R. D., Mazeh, T., & Vrba, F. J. 1999, AJ, 117, 2941

Sullivan, P. W., Winn, J. N., Berta-Thompson, Z. K., et al. 2015, ApJ, 809, 77

Tokovinin, A., Thomas, S., Sterzik, M., & Udry, S. 2006, A&A, 450, 681

Torres, G., Curtis, J. L., Vanderburg, A., Kraus, A. L., & Rizzuto, A. 2018, ApJ, 866, 67

Van Eylen, V., Winn, J. N., & Albrecht, S. 2016, ApJ, 824, 15

van Saders, J. L., Pinsonneault, M. H., & Barbieri, M. 2018, ArXiv e-prints, arXiv:1803.04971

Verbunt, F., & Zwaan, C. 1981, A&A, 100, L7

Witte, M. G., & Savonije, G. J. 2002, A&A, 386, 222

Zahn, J.-P. 1994, A&A, 288, 829

Zahn, J.-P. 2008, in EAS Publications Series, Vol. 29, EAS Publications Series, ed. M.-J. Goupil & J.-P. Zahn, 67–90

Zahn, J.-P., & Bouchet, L. 1989, A&A, 223, 112